Infrared studies of the energy gap in tetrathiofulvalene-tetracyanoquinodimethane (TTF-TCNQ)

D. B. Tanner,* C. S. Jacobsen,† A. F. Garito, and A. J. Heeger

Department of Physics and Laboratory for Research on the Structure of Matter,‡ University of Pennsylvania, Philadelphia, Pennsylvania 19174

(Received 1 May 1975)

Infrared studies of single crystals and thin films of the one-dimensional organic metal tetrathiofulvalene-tetracyanoquinodimethane (TTF-TCNQ) are presented. The frequency-dependent conductivity, $\sigma_1(\omega)$, and dielectric function, $\epsilon_1(\omega)$, are obtained by Kramers-Kronig analysis of the single-crystal reflectivity. The results indicate the existence of an energy gap ($E_g = 0.14$ eV) in the optical spectrum. Transmission and reflection measurements on sublimed thin films of TTF-TCNQ yield results for the response functions in excellent agreement with those obtained from single crystals. The thin-film data are presented for several temperatures, both above and below the metal-insulator transition. The energy gap is present at all temperatures; reduction of the temperature sharpens the structure, but the metal-insulator transition is all but invisible at these frequencies. At low temperatures the overall level of the conductivity in the far infrared decreases as the pinned collective mode appears, centered in all films measured to date at 80 cm^{-1}. The data are analyzed in terms of a simple two-fluid model described by a collective mode and a single-particle excitation spectrum. Quantitative estimates of the collective-mode oscillator strength, $\Omega_p \simeq 500$ cm^{-1}, effective mass, $M^* \simeq 300\,m^*$, where the band mass is $m^* \simeq 3\,m_e$, and lifetime, $\tau_c^{-1} \simeq 0.5$ cm^{-1} near 60 K, are obtained from the infrared conductivity and dielectric functions. A consistent picuture of TTF-TCNQ is developed in terms of a Peierls-Fröhlich conductor with the Peierls gap established and the Fröhlich mode sliding at temperatures above 58 K and pinned at temperatures below 58 K.

I. INTRODUCTION

This paper presents the results of an extensive study of the infrared properties of tetrathiofulvalene-tetracyanoquinodimethane (TTF-TCNQ). The central feature is the existence of an energy gap ($\hbar\omega_g = 0.14$ eV) in the infrared conductivity which is present at all temperatures studied.[1,2] Taken together with previous work on the dc electrical conductivity,[3-6] microwave conductivity and dielectric constant[7-10] near infrared and optical reflectance,[11-13] magnetic susceptibility,[14] specific heat,[15,16] and x-ray diffraction,[17] these results allow a reasonably consistent picture to be drawn of TTF-TCNQ in terms of a Peierls-Fröhlich[18,19] conductor with the Peierls[18] gap established and the Fröhlich mode[19] sliding at temperatures above 58 K and pinned[20,21] at temperatures below 58 K.

The early suggestion[3] of superconductive fluctuation phenomena in TTF-TCNQ was based on the existence of the relatively large and strongly temperature-dependent dc electrical conductivity. The existence of high conductivities in pseudo one-dimensional systems is necessarily a many-body effect resulting from attractive electron-electron interactions. For example, Bychkov,[22] Berezinskii,[23] and Gagolin, Mel'nikov, and Rashba[24] have shown rigorously that, for independent electrons in a strictly one-dimensional (1D) system containing impurities or defects, the conductivity decreases as the temperature is lowered, approaching zero with a temperature dependence determined by the ratio of the impurity and phonon scattering rates, $\tau_{imp}/\tau_{ph}(T)$.

The early suggestion[3] that the electron-electron correlations in TTF-TCNQ are mediated by soft phonons near $2k_F$ led Bardeen[25] to point out that, although the correlations might indeed result from the Peierls instability, the resultant lattice distortion need not be static with fixed phase from chain to chain but dynamic, giving rise to giant density waves in the solid. Fröhlich[19] first demonstrated that coupling of the electron to these giant density waves in 1D systems can lead to superconductive behavior. In effect, the electrons "surf-ride" on the giant density waves in the underlying lattice, and electron scattering is inhibited by the strong coupling of the electron-lattice system. Because of the absence of long-range order in one-dimensional systems and the existence of dissipative processes for the giant density-wave mechanism, one can expect large enhanced conductivities but not true persistent currents.

It is useful to look at the Fröhlich state from an energy-band point of view. Following Allender, Bray, and Bardeen,[26] we show in Fig. 1 an idealized $\epsilon(k)$ vs k for a one-dimensional tight-binding metal with zero current [1(a)] and with a finite current [1(b)]. The fact that the energy gap is tied to the Fermi surface in the moving frame of reference suppresses single-particle back scattering across $2k_F$ and gives rise to enhanced conductivity. In the actual system, as a result of the one-dimensional fluctuations which are present above the three-dimensional interchain ordering temperature, the energy gap becomes a pseudogap; but at least schematically the same ideas

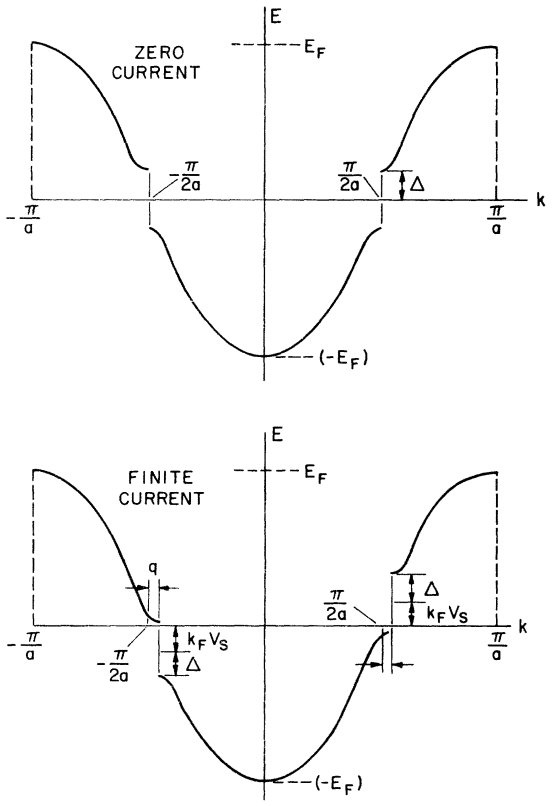

FIG. 1. Band structure of the Peierls-Frohlich conductor. (a) Zero current; (b) finite current showing the shift in the energy gap.

apply.

Figure 1 suggests the existence of two kinds of electronic excitations in such a Peierls-Fröhlich conductor.

(i) A collective mode of the coupled electron-lattice system: Since the Peierls-Fröhlich state can be viewed as a coherent superposition of polarons, it is not surprising that the collective mode has a large effective mass M^* dominated by the electron-phonon coupling.[19] In addition, since the many-body collective behavior suppresses scattering, one anticipates an extremely long collective-mode scattering time τ_c.

(ii) Single-particle excitations across the pseudo-gap: These are analogous to the simple excitations in a semiconductor and correspond to shake-off excitations in which an electron is excited, leaving the underlying lattice fixed. The single-particle excitations should have the simple band mass m^* and a relatively short single-particle scattering time τ_{sp}.

Schrieffer[20] and Lee, Rice, and Anderson,[21] have pointed out the extreme sensitivity of the Fröhlich giant density-wave mechanism to pinning. The physical point is that charged impurities, defects, and intrinsic interchain coupling all conspire to fix the phase of the collective mode and thereby pin it and inhibit motion. In this case, the pinning effects provide a restoring force to the collective-mode motion and shift the collective-mode oscillator strength from zero frequency to a finite pinning frequency ω_T.

Based on the above considerations, one can construct a schematic diagram of $\sigma_1(\omega)$ vs ω showing the characteristic features of the collective mode and single-particle excitations as shown in Fig. 2. In the conducting state [Fig. 2(a)] the collective mode is centered at zero frequency, with a width determined by the collective-mode lifetime $\tau_c(T)$. The energy gap leads to a broad minimum in $\sigma_1(\omega)$ with the single-particle (semiconductor interband) transitions showing up at higher frequencies. When the frequency exceeds the single-particle scattering rate, the usual Drude roll-off $[\sigma_1(\omega) = (Ne^2/m^*)/\omega^2\tau_{sp}]$ is expected. Pinning of the collective mode will shift the oscillator strength into the infrared and probably broaden it considerably [Fig. 2(b)].

The fundamental signature of the Fröhlich state

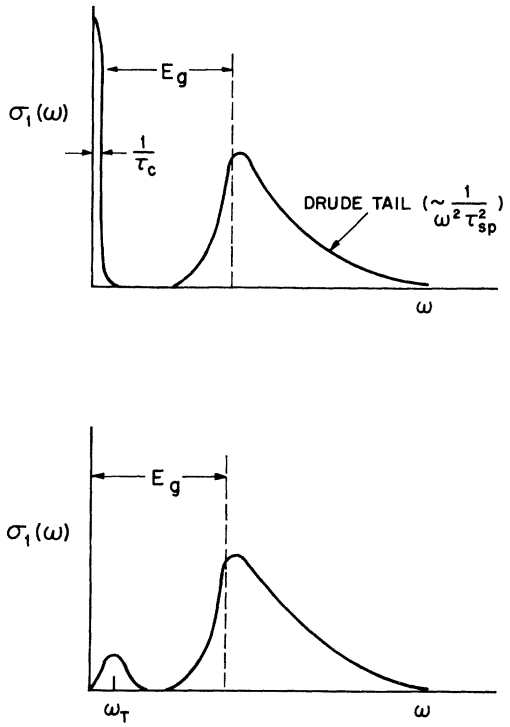

FIG. 2. Schematic representation of the frequency-dependent conductivity of the Peierls-Frölich conductor showing the collective-mode peak and the single-particle oscillator strength at higher frequencies. (a) Conducting state with collective mode centered at zero frequency. (b) Insulating state, with the collective mode pinned at a low frequency.

is, therefore, relatively high electrical conductivity, $\sigma_F = N_F e^2 \tau_c / M^*$, in the presence of a pseudogap in the electronic excitation spectrum. The high conductivity is expected to be extremely sensitive to pinning by defects and impurities. At sufficiently low temperature, interchain Coulomb coupling of the charge-density waves or 3D band structure effects will cause a three-dimensional ordering transition at which point the phase of the charge-density wave is pinned, leading to a high dielectric constant insulating state. These are precisely the features observed in the frequency-dependent condutivity and dielectric function of TTF-TCNQ.

Besides the theoretical work discussed above, there have been a number of microscopic calculations of the conductivity of one-dimensional systems. Many of the issues have not been resolved at this time. Luther and Peschel[27] have calculated the conductivity in the Tomonaga model exactly for small momentum transfer. They obtain large fluctuation enhancements of the conductivity. Similar results were reported by Mattis.[28] Fukuyama, Rice, and Varma,[29] on the other hand, find, in a calculation where impurities are the only momentum-dissipation mechanism, that fluctuations enhance the resistivity not the conductivity. The effects that lead to pinning in the ordered state give a resistivity enhancement in the fluctuation regime. Patton and Sham[30] also get a resistivity enhancement in the case where the Peirels's distortion is commensurate with the lattice. However, in the incommensurate case, including random impurities, Patton and Sham[31] find that phonon-drag terms lead to an enhanced fluctuation conductivity. The pinning term has no effect above the temperature where the ordered state sets in. Sokoloff[32] finds that weak impurities do not always pin the charge-density wave, which distorts to accomodate the impurity. In effect, near the impurity the charge-density wave is made up of a superposition of the undistorted wave and a localized impurity mode so as to minimize the energy of interaction with the impurity. Rice[33] has made a semiphenomenological calculation of the conductivity due to the sliding mode and finds the conductivity increasing as the temperature is reduced with maximum values for TTF-TCNQ on the order of 10^4–10^5 $\Omega^{-1}\,\mathrm{cm}^{-1}$. The final resolution of these theoretical studies is not yet clear. Therefore, our point of view in this paper will be to continue to develop detailed experimental data on $\sigma_1(\omega)$ and $\epsilon_1(\omega)$ and to compare the results with the phenomenological model of the Peierls-Fröhlich state.

Short communications on the infrared conductivity of TTF-TCNQ films[1] and single crystals[2] have been published by us earlier. Torrance and Nicoli[34] measured the absorption of TTF-TCNQ powders dispersed in KBr and in polyethylene and have obtained curves for the conductivity which are, in their major features, in agreement with our results. Chaudhari *et al.*[35] have measured the infrared and visible transmission of oriented TTF-TCNQ films and obtained results similar to those here. Poehler *et al.*[36] have measured the polarized response of a single crystal to a number of lines from a far-infrared laser and found at 4.2 K an increase in absorption at 220 cm^{-1} (0.03 eV), which they attributed to photoconductivity across a small gap associated with the 58 K metal-insulator transition. This edge will be seen here to be present at all temperatures below 320 K and to be nearly independent of temperature. Eldridge[37] has measured the bolometric response of a single crystal to a Michelson interferometer and found at 7 K many more optical-phonon modes than expected, a strong absorption edge beginning at 320 cm^{-1}, and a broad asymmetric peak at 7 cm^{-1} which he attributes to a pinned Fröhlich mode.

The plan of the paper is as follows: In Sec. II, sample preparations and infrared experimental techniques are described. Section III presents room-temperature (300 K) polarized reflectance studies of single crystals of TTF-TCNQ, which are analyzed via a Kramers-Kronig scheme to obtain $\sigma_1(\omega)$ and $\epsilon_1(\omega)$ for both the b and a crystallographic directions. Section IV describes the data obtained on sublimed thin films at temperature from 5 to 320 K. Transmission and reflection measurements on the same specimen are analyzed to obtain $\sigma_1(\omega)$ and $\epsilon_1(\omega)$. This section also contains a discussion of the importance of small particle depolarization effects. Section V discusses a fit to the data using a Lorentzian oscillator and Drude relaxation time. The oscillator strength sum rule is used to obtain an estimate of the effective mass of the electrons, and a discussion of the plasma edge in terms of the loss function is given. Section VI describes the data in the context of the Peierls-Fröhlich model and of the Lee, Rice, and Anderson concept of pinning of the collective mode. We are led to a simple two-fluid model and give an estimate of the oscillator strength, effective mass, and lifetime of the collective mode. In Sec. VII we consider deviations of the measured conductivity from a Drude-Lorentz model and calculate the frequency dependence of a complex relaxation rate. Section VIII is a summary.

There are a number of complex functions of frequency which describe the response of matter to electromagnetic waves, such as the complex index of refraction N, conductivity σ, and dielectric function ϵ. All of these are related to one another.

In this paper, we have chosen to always present the data as the real part of the conductivity $\sigma_1(\omega)$ and as the real part of the dielectric function $\epsilon_1(\omega)$, since these are the quantities measured at zero frequency. They are related via the Kramers-Kronig integral transforms

$$\epsilon_1(\omega) = 1 + 8P\int_0^\infty \frac{\sigma_1(\omega_1)\,d\omega_1}{\omega_1^2 - \omega^2}, \tag{1}$$

and can be written together as the complex conductivity

$$\sigma(\omega) = \sigma_1(\omega) - i(\omega/4\pi)[\epsilon_1(\omega) - 1]$$

or complex dielectric function

$$\epsilon(\omega) = \epsilon_1(\omega) + i(4\pi/\omega)\sigma_1(\omega).$$

II. MATERIALS AND INFRARED TECHNIQUES

High-purity TTF and TCNQ were prepared by methods similar to those described earlier.[4,7,12,38] The products were purified by multiple gradient sublimation and handled in inert Ar (99.999%) atmosphere.

TTF-TCNQ single crystals were grown by diffusion in a solution of ultrapure acetonitrile using a specially designed vessel and programmed temperature control. The crystals grow in the form of flat needles with the long axis of the crystal coincident with the principal conducting (crystallographic b) axis of the solid. The largest crystal face contains the crystallographic a-b plane. With careful selection, crystals can be obtained with excellent surfaces suitable for optical reflectivity experiments.

In addition to single crystals, polycrystalline films were used in this study. The films were prepared by vacuum sublimation of the high-purity salt TTF-TCNQ. The sublimation was carried out at temperatures in the range (80–110) °C in a Varian high-vacuum evaporator at pressures below 2×10^{-5} Torr using a tantalum boat. The source to substrate distance was chosen (for convenience) to be 5 cm, and the substrates were held at 10 °C by attaching them to a water-cooled copper block. Known amounts of TTF-TCNQ were used, and the film thicknesses were obtained to an accuracy of ±25% from the source-substrate configuration. Thinner films under transmitted light exhibited the yellow-brown color characteristic of pure TTF-TCNQ and a matte finish; thicker films were flat black. Scanning electron micrographs showed that the films consisted of many small well-formed single crystals, with typical dimensions $3\times0.5\times0.1$ μm^3, growing on the substrate with random orientation. Debye-Scherrer x-ray patterns showed the films had crystallized in the bulk structure, and chemical analysis confirmed the 1:1 TTF-TCNQ salt.

Substrates and film thickness were chosen to give reasonable transmission at all frequencies. Measurements in the range 20–350 cm^{-1} were performed on 1–2-μm-thick films grown on sapphire, Mylar, and polyethylene, while 2000–3000-Å-thick films on KBr were used from 300 to 4000 cm^{-1}.

Infrared spectra were recorded using a Perkin-Elmer 225 spectrophotometer over the region 300–5000 cm^{-1}, and a Grubb-Parsons-Michelson interferometer over the region 20–500 cm^{-1}. The Perkin-Elmer 225 is a double beam grating instrument using a Golay cell detector and is equipped with a gold wire grid polarizer. The low-temperature measurements on this instrument were made using an Air Products Helitran cryotip with CsI windows. The reflectance measurements employed a Perkin-Elmer microspecular reflectance insert, which gives an angle of incidence of approximately 10° from the normal to the crystallographic a-b plane, in the a-c^* plane.

The Michelson interferometer had a gallium-doped germanium bolometer-detector operating at 1.2 K. The detector Dewar employed standard light-pipe optics with the sample mounted on a rotating disc. The reflectance insert used is shown in Fig. 3. Just above the sample is a beam splitter which consists of a mitered right-angle bend with a hole drilled in the brass mirror. The beam splitter passes part of the incident radiation to the sample and reflects part of the return to the adjacent mitered corner whence it passes on to the detector. Both a sample and a reference mirror are attached to the copper rotator disc (along with

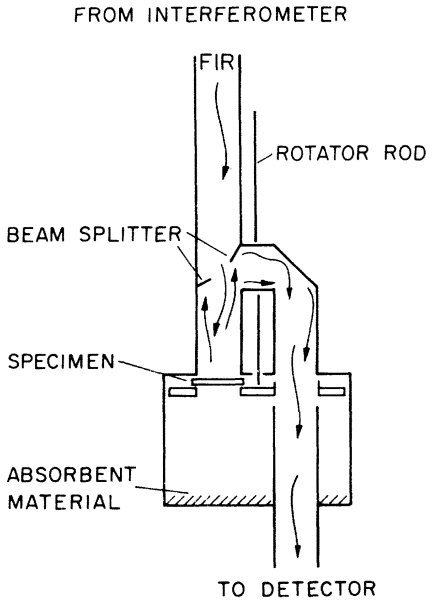

FIG. 3. Far-infrared reflectance insert.

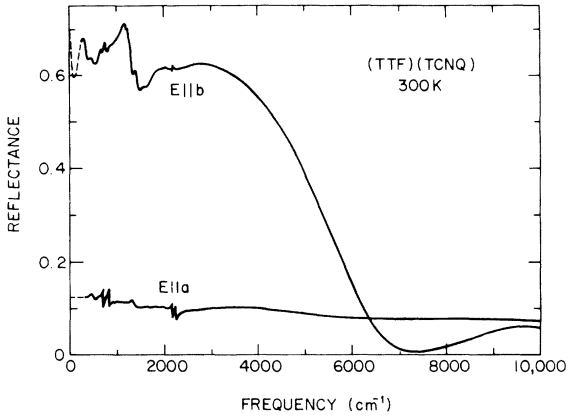

FIG. 4. Polarized reflectance of TTF-TCNQ single crystals over the whole region, 50–10 000 cm^{-1}. The dashed lines below 350 cm^{-1} indicate data derived from the unpolarized reflectance of an oriented mosaic.

a thermometer and heater for temperature control) and either may be placed in the beam. The actual rig has the sample and the clear hole located 90° apart rather than 180°, as shown in the figure, so that the rotator rod can pass by on axis. This insert is expected to show an insertion loss of a factor of 4 (2 at each incidence on the beam splitter); the measured loss is a factor of 5. There is considerable leakage or stray reflection; with no sample mounted, the signal at the detector is 30% of that from a mirror. The raw data are corrected for this background before further analysis.

III. SINGLE-CRYSTAL REFLECTANCE

The measurements were performed on single crystals, approximately 2×10 mm^2, using as grown surfaces. Figure 4 shows the polarized reflectance at room temperature for $E \parallel b$ and $E \parallel a$ in the range 50–10 000 cm^{-1}. The dashed lines in the range 50–300 cm^{-1} were obtained from unpolarized reflectance from a carefully aligned mosaic of single crystals mounted on thin gold wires. The individual crystals were again approximately 2×10 mm^2, and five or six were used to fill the far-infrared beam. $\mathcal{R}(E \parallel b)$ is obtained by assuming $\mathcal{R}(E \parallel a)$ is constant at the 300 cm^{-1} value so that $\mathcal{R}(E \parallel b) = 2\mathcal{R}_{meas} - \mathcal{R}(E \parallel a)$.

$\mathcal{R}(E \parallel a)$ is essentially frequency independent except for several sharp resonances which are identified as arising from various intramolecular vibrations.

$\mathcal{R}(E \parallel b)$ is less than 72% throughout the intermediate-infrared regime. A broad resonant structure is seen around 1200 cm^{-1} in addition to diverse sharp resonances from molecular vibrations and possibly lattice phonons. $\mathcal{R}(E \parallel b)$ remains considerably below the values that would be expected from a simple metal with a dc conductivity of 500–1000 $\Omega^{-1}\,cm^{-1}$ and a well-shaped plasma edge at 7000 cm^{-1}.[11–13] The relatively low reflectance values at long wavelengths thus imply an energy gap $E_g = \hbar\omega_g$ with $\omega_g\tau_{sp} \sim 1$ where τ_{sp} is the single-particle scattering time appropriate to excitations near the gap edge.

Since the polarized reflectance is known for frequencies up to 37 000 cm^{-1} a Kramers-Kronig analysis[2,39] is expected to give reliable results in the infrared regime. We have used data from our measurements between 50 and 5000 cm^{-1}; the data of Bright *et al.*[12] between 5000 and 10 000 cm^{-1}; and the data of Grant *et al.*[13] between 10 000 and 37 000 cm^{-1}. Beyond these frequencies conventional extrapolation schemes were employed. In the range $0 < \omega < 50$ cm^{-1} it was assumed either that $\mathcal{R}(E \parallel b)$ behaves according to the Hagen-Rubens formula $\mathcal{R} = 1 - (2\omega/\pi\sigma)^{1/2}$ with $\sigma \simeq 60$ $\Omega^{-1}\,cm^{-1}$, chosen so a smooth connection with the data was obtained, or that $\mathcal{R}(E \parallel b)$ was constant. The value for $\mathcal{R}(E \parallel a)$ was assumed constant in this limited low-frequency range.

The high-frequency extrapolation must simulate interband transitions and, at very high frequencies, free-electron behavior. For the b-axis data, we have used the standard approximation $\mathcal{R}(\omega) = \mathcal{R}(\omega_c) \times (\omega_c/\omega)^P$ with $\omega_{c1} = 37\,000$ cm^{-1}, $P_1 = 2$ (corresponding to interband transitions), $\omega_{c2} = 200\,000$ cm^{-1}, and $P_2 = 4$ (corresponding to free-electron behavior). The a-axis high-frequency extrapolation was chosen to give the best agreement with the measured a-axis absorption coefficient of Bright *et al.*[12] as discussed below.

The sensitivity to the choice of extrapolation procedures is illustrated by the following examples: Assuming $\mathcal{R}(E \parallel b)$ constant for $\omega < 50$ cm^{-1} leads to changes in σ and ϵ of less than 2% for $\omega > 500$ cm^{-1} and yields even lower values for σ (the dotted curve in Fig. 5 below 200 cm^{-1}) than the Hagen-Rubens extrapolation (the dashed curve below 200 cm^{-1}) in the gap region. Thus the data above 200 cm^{-1} are insensitive to the detailed low-frequency extrapolation procedure. Assuming constant reflectance above 37 000 cm^{-1} leads to changes less than 10% for any $\omega < 10^4$ cm^{-1} and has negligible effect below 500 cm^{-1}.

The frequency-dependent conductivity $\sigma_1(\omega)$ and dielectric function $\epsilon_1(\omega)$, as obtained from the Kramers-Kronig analysis, are shown for $E \parallel b$ and $E \parallel a$ in Figs. 5–11.

The main feature in σ_1^b (Fig. 5) is a resonant structure with an absolute maximum at approximately 1100 cm^{-1}, with a strong relatively narrow minimum centered at approximately 1400 cm^{-1}. At higher frequencies a smooth Drude-like frequency dependence is observed.

Figures 6 and 7 show the single-crystal $\sigma_1^b(\omega)$ data over a broader spectral range. The Drude-

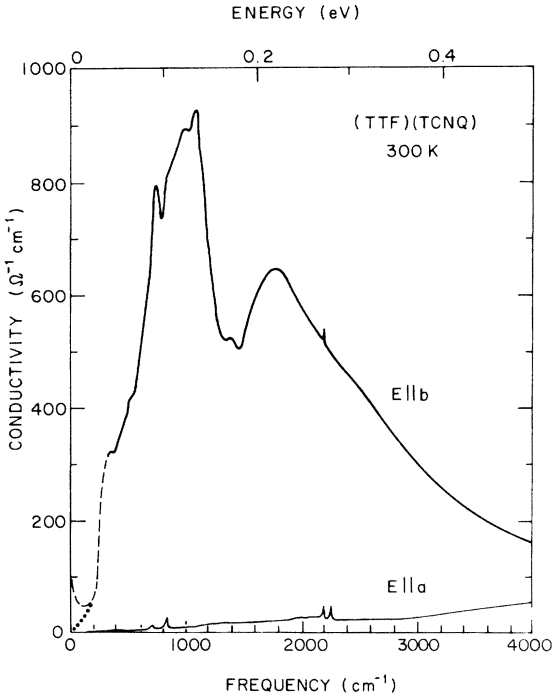

FIG. 5. Real part of the conductivity of TTF-TCNQ single crystals for both $E \parallel b$ and $E \parallel a$ vs frequency from 20–4000 cm^{-1}. The dashed and dotted curves at low frequencies indicate two different extrapolation procedures.

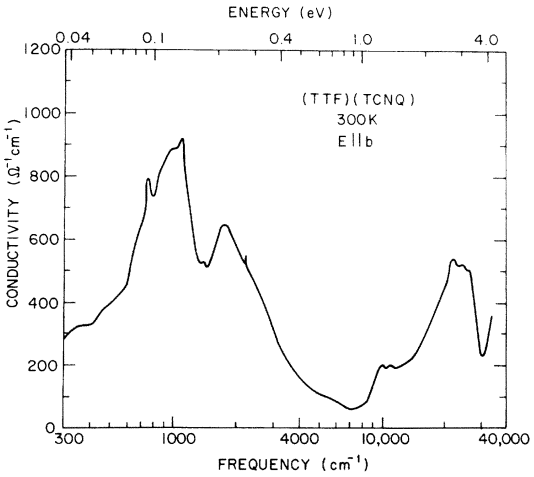

FIG. 7. Real part of the conductivity of TTF-TCNQ single crystals for $E \parallel b$ vs frequency from 300–37 000 cm^{-1}. The frequency scale is logarithmic.

like regime (2000–8000 cm^{-1}) is interrupted by the onset of absorption at 9000 cm^{-1}, probably due to excitonic or interband transitions.

The corresponding behavior of ϵ_1^b (Figs. 8 and 9) is that of an insulator with a resonance sufficiently strong to give negative values between 1000 and 6000 cm^{-1}. At lower frequencies ϵ_1^b is quite high

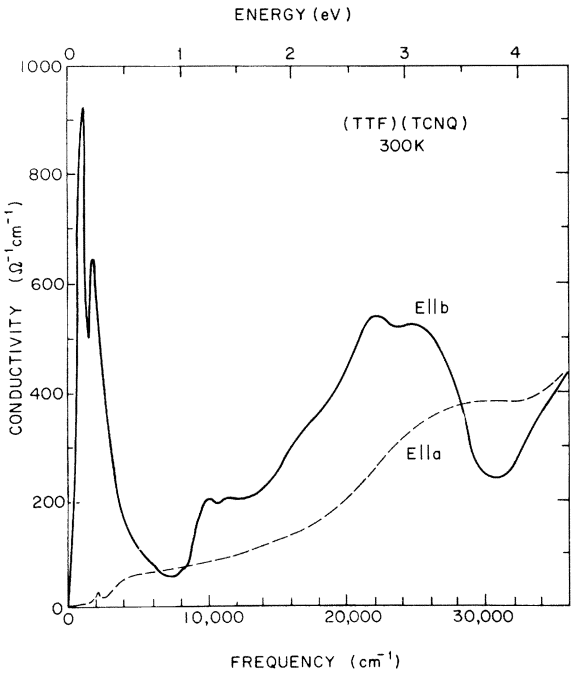

FIG. 6. Real part of the conductivity of TTF-TCNQ single crystals for both $E \parallel b$ and $E \parallel a$ vs frequency from 20–37 000 cm^{-1}.

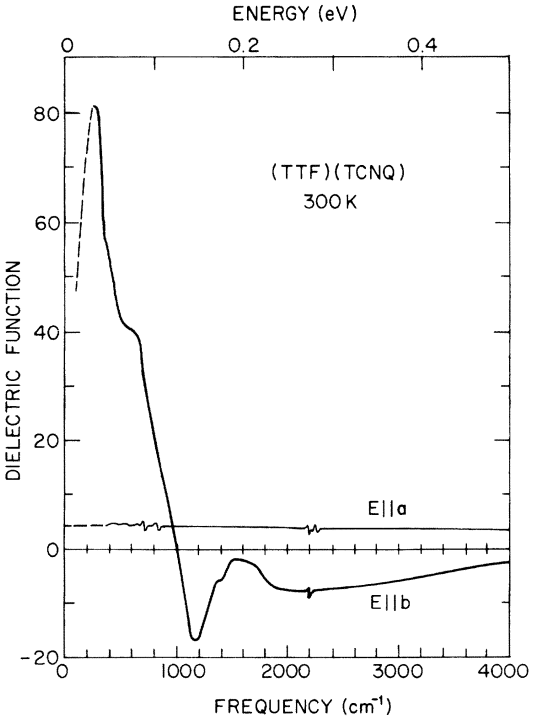

FIG. 8. Real part of the dielectric function of TTF-TCNQ single crystals for both $E \parallel b$ and $E \parallel a$ vs frequency from 20–4000 cm^{-1}.

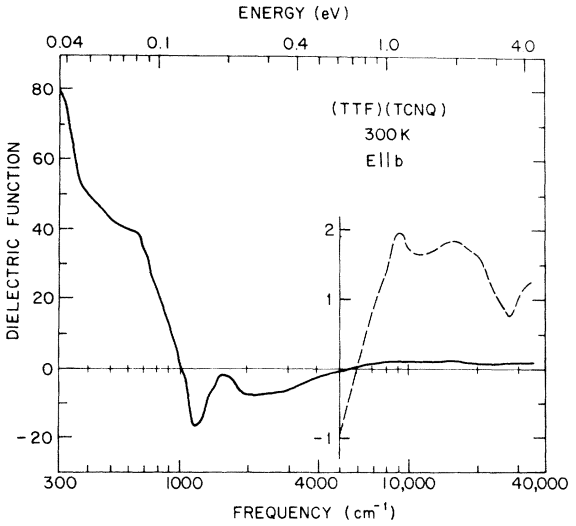

FIG. 9. Real part of the dielectric function of TTF-TCNQ single crystals for $E \parallel b$ vs frequency from 300–37 000 cm^{-1}. Notice the logarithmic frequency scale. The dashed curve at high frequencies shows the data magnified by a factor of 20.

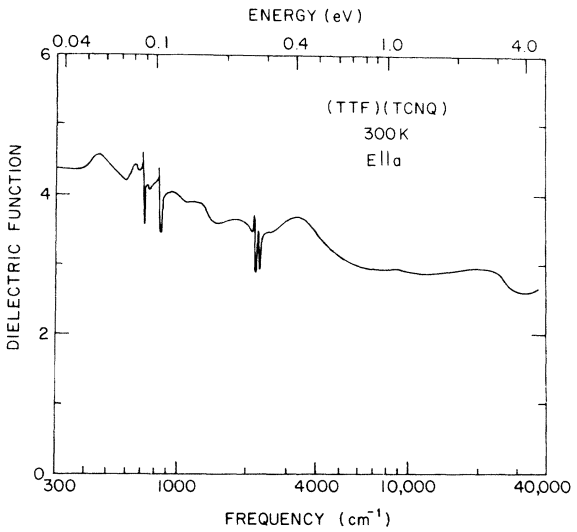

FIG. 11. Real part of the dielectric function of TTF-TCNQ single crystals for $E \parallel a$ vs frequency from 300–37 000 cm^{-1}. The frequency scale is logarithmic.

with a maximum value of 82 near 300 cm^{-1}, while the dielectric behavior in the far infrared is not known directly. The existence of large dc and microwave conductivities ($\sigma^b_{dc} = \sigma^b_{\mu wave} \simeq 10^3\ \Omega^{-1}\,cm^{-1}$) implies that $\epsilon_1^b(\omega)$ crosses zero and is negative at very low frequencies.

The a-axis conductivity and dielectric function are shown in Figs. 5, 6, 8, 10, and 11. The main features are the molecular lines and the absence of any sign of metallic behavior. The frequency-dependent conductivity remains small and increases slowly out to approximately 10^4 cm^{-1}. At the highest frequencies, where the intramolecular transitions dominate, the a-axis and b-axis conductivities become comparable. ϵ_1^a (Fig. 11) is falling off slowly from 4.5 to approximately 3 with increasing frequency. The contributions from the various sharp molecular modes are seen clearly. There is no C-H stretching mode. These measurements were made on TTF-TCNQ:D8 crystals because of their large size.

The extrapolation procedure at high frequencies for the a direction was chosen to give the best possible agreement between the calculated and measured absorption coefficient in the visible. The absorption coefficient $\alpha = 2k\omega/c$ is shown for the two directions in Fig. 12. The directly measured single-crystal a-axis absorption of Bright *et al.*[11,12] (in the visible part of the spectrum) is also shown in the figure.

The data of Bright *et al.*[11,12] (and the color of thin crystals under transmitted light with $E \parallel a$) show a strong increase of absorption for $E \parallel a$ at frequencies above 25 000 cm^{-1} (3.5 eV). The reflectance data of Grant *et al.*[13] is, however, quite smooth in this region accounting for the less steep rise in the absorption coefficient derived from the Kramers-Kronig transform. The absorption coefficient for $E \parallel b$ is in reasonable agreement with the data of Chaudhari *et al.*[35] on epitaxial films.

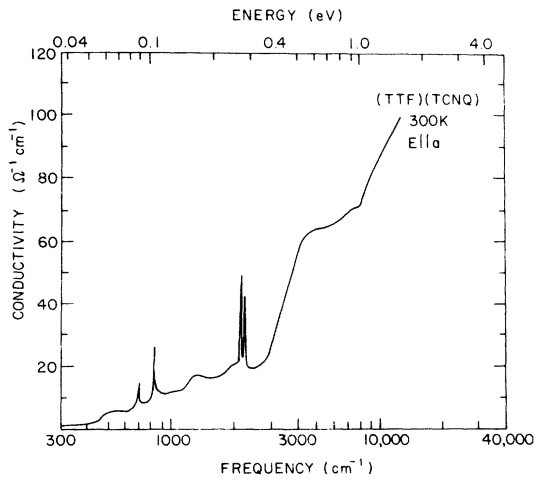

FIG. 10. Real part of the conductivity of TTF-TCNQ single crystals for $E \parallel a$ vs frequency from 300–37 000 cm^{-1}. Notice the logarithmic frequency scale.

IV. THIN-FILM DATA

In this section we present the data obtained from measurements on thin films of TTF-TCNQ. Figures 13 and 14 show the absorption coefficient α uncorrected for reflection. This is given by

$$\alpha = -(1/d)\ln I/\mathcal{T}_{sub},$$

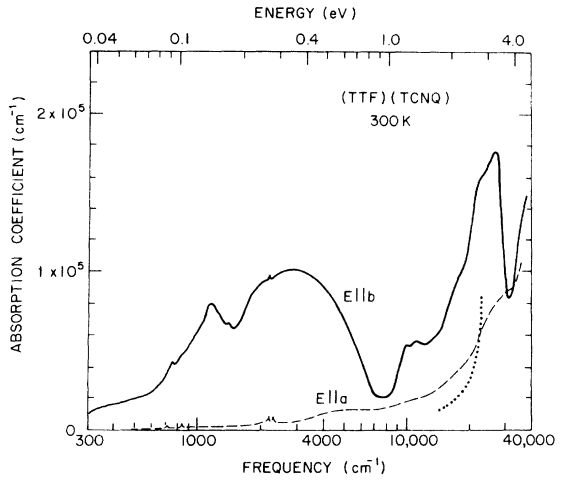

FIG. 12. Absorption coefficient of TTF-TCNQ single crystals for $E \| b$ and $E \| a$ vs frequency from 300–37 000 cm^{-1}. These data are derived from the complex conductivity. The dotted line is the measured absorption coefficient for $E \| a$ for a thin single crystal (see Ref. 10).

where d is the film thickness in cm, $\mathcal{T}$ is the transmission of a film on a substrate, and $\mathcal{T}_{sub}$ is the transmission of the uncoated substrate. The absorption coefficient is not a particularly well-defined quantity in the present case, since the film thickness is less than the wavelength or skin depth, so that the infrared intensity does not decay in any exponential way while passing through the film. It does, however, provide a qualitative measure of the excitation spectrum in the film.

Figure 13 shows the absorption coefficient at three temperatures for frequencies between 30 and 4000 cm^{-1}. Data in the range above 300 cm^{-1} are from films grown on KBr, 200–300 cm^{-1} from films grown on Mylar, and 30–200 cm^{-1} from films

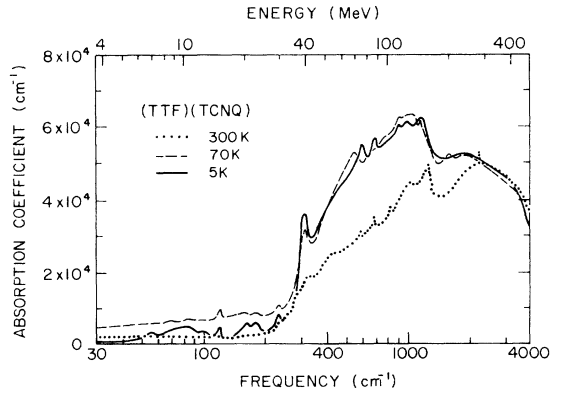

FIG. 13. Absorption coefficient of TTF-TCNQ films at three temperatures vs frequency from 30–4 000 cm^{-1}. The frequency scale is logarithmic. The weak absorption at low frequencies indicates an energy gap.

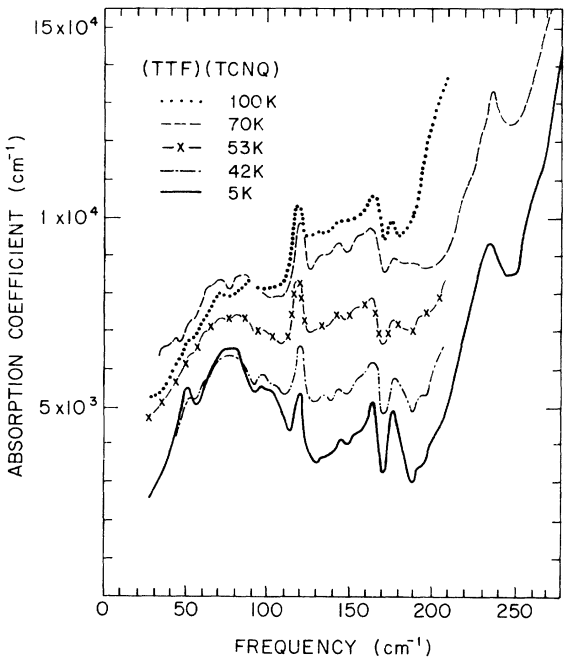

FIG. 14. Absorption coefficient of a TTF-TCNQ film on sapphire at five temperatures vs frequency from 20–270 cm^{-1}.

grown on sapphire (5 and 70 K) and polyethylene 70 and 300 K). Note that the absorption coefficient between 300 and 4000 cm^{-1} at room temperature is quite similar to that obtained from the single-crystal measurements.

There are maxima at 1250 and 2400 cm^{-1} with an increase of nearly an order of magnitude between 200 and 1000 cm^{-1}. At lower temperatures the edge becomes much steeper and somewhat stronger. The steep onset of the absorption coefficient at 250 cm^{-1} separates rather neatly two infrared regions. In the middle infrared (250–4000 cm^{-1}) there is high absorption and the structure associated with the conductivity reaches a maximum near 1000 cm^{-1}. On cooling from 300 to 65 K the absorption coefficient is substantially increased, while further cooling to 5 K makes very little difference. In the far infrared (30–250 cm^{-1}) the absorption coefficient is much lower and, while cooling from 300–65 K gives a large increase in absorption coefficient, reduction of the temperature to 5 K decreases the absorption while a broad maximum appears around 80 cm^{-1}. The low-frequency and low-temperature data are shown in more detail in Fig. 14 which gives the absorption coefficient of a TTF-TCNQ film on sapphire between 25 and 280 cm^{-1} for five temperatures between 5 and 100 K. As the temperature is increased the over-all strength of the absorption is increased and the broad maximum seen at 80 cm^{-1} at 5 K becomes progressively weaker. Also seen

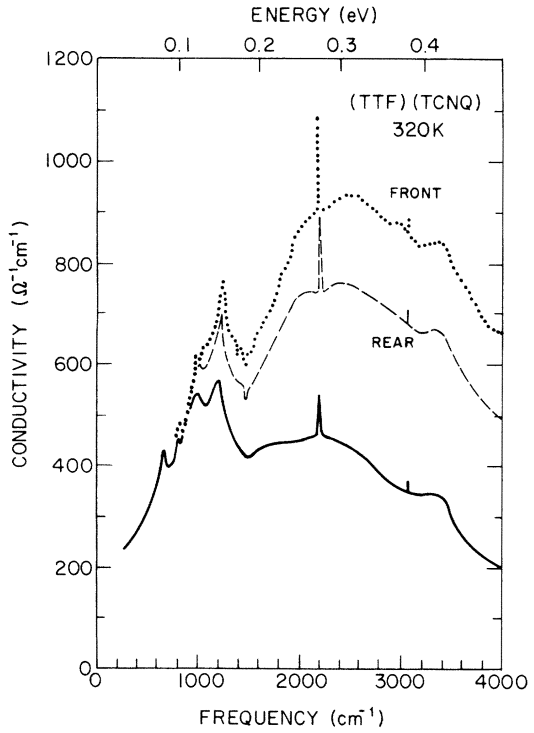

FIG. 15. Real part of the conductivity of a TTF-TCNQ film on KBr at room temperature vs frequency from 300–4000 cm^{-1}. The dotted and dashed curves illustrate the difficulties caused by scattering: the solid curve includes the scattering correction.

on Fig. 14 are a number of sharp absorption lines. Most noticeable are temperature-independent lines at 119 and 234 cm^{-1} and temperature-dependent lines at 51, 163, and 178 cm^{-1}.

The complex conductivity $\sigma = \sigma_1 - (i\,\omega/4\pi)(\epsilon_1 - 1)$ may be determined from normal-incidence measurements of the reflectance and transmittance of a film. This was done for superconductors in the far infrared by Palmer and Tinkham.[40] The problem of finding the reflectance and transmittance of a film on a substrate is a relatively straightforward, if tedious, boundary-value problem which has been solved by a number of authors interested in interference filters. The clearest paper we know of is by Hadley and Dennison.[41] The solution can be very simple if the film is thin with respect to its skin depth and the wavelength of the light, since it may then be obtained from the boundary conditions on the field vectors, treating the film as a sheet of surface current.[42] The results for the transmittance and reflectance of the film are

$$\mathcal{T}_F = \frac{4n_1 n_2}{[n_1 + n_2 + (4\pi/c)\sigma_1 d]^2 + [(\omega/c)(\epsilon_1 - 1)d]^2}, \quad (2)$$

$$\mathcal{R}_F = \frac{[n_2 - n_1 + (4\pi/c)\sigma_1 d]^2 + [(\omega/c)(\epsilon_1 - 1)d]^2}{[n_1 + n_2 + (4\pi/c)\sigma_1 d]^2 + [(\omega/c)(\epsilon_1 - 1)d]^2}, \quad (3)$$

where d is the film thickness, n_1 is the index of refraction of the medium in which the incident and reflected radiation is traveling, and n_2 is the index of the medium in which the transmitted wave is traveling. Notice that the expression for the reflectance is changed by interchange of n_1 and n_2 (turning the specimen over). After corrections for absorption within the substrate and for effects of the uncoated side of the substrate, including multiple internal reflections, $\sigma_1(\omega)$ and $|\epsilon_1(\omega) - 1|$ can be calculated from the measured external transmittance and reflectance.

Figure 15 shows the real part of the conductivity over the frequency range from 300 to 4000 cm^{-1}. Since the films are composed of randomly oriented crystallites, we have plotted $3\langle\sigma_1\rangle$ where $\langle\sigma_1\rangle$ is the conductivity calculated as described above. Since $\sigma_1^a \ll \sigma_1^b$ (and presumably the same is true for σ_1^c), the quantity $3\langle\sigma_1\rangle$ corresponds to the b-axis conductivity. This allows direct comparison with the single-crystal results. The dotted line gives the result of using the transmittance and reflectance with the radiation incident on the exposed front surface, and the dashed line gives the result obtained from transmittance and reflectance with the radiation incident through the substrate on the rear surface. The two curves are similar at low frequencies but begin to separate at about 900 cm^{-1}, with the relative differences becoming large as the frequency increases.

As the matte appearance of the films under visible light suggests, the problem is caused by scattering. This was quantitatively demonstrated by a sample tipping experiment performed at 4000 cm^{-1}. A TTF-TCNQ film and a gold mirror were placed in the reflectance attachment of the Perkin-Elmer and progressively tipped away from the specular reflectance position. As shown in Fig. 16, the signal from the gold mirror cuts off at the 6° acceptance half angle of the instrument as expected, while that from the TTF-TCNQ film has an average value of 2% through the next 8°. This leads to a direct estimate that the fraction of the radiation that is nonspecularly reflected is, at 4000 cm^{-1}, 50% of the amount specularly reflected.

We adopt the following scheme to correct for the scattering. By conservation of energy

$$\begin{aligned} &\mathcal{T}_F + \mathcal{R}_F + \mathcal{A}_F = 1 \quad \text{(front)}, \\ &\mathcal{T}_F + \mathcal{R}'_F + \mathcal{A}'_F = 1 \quad \text{(rear)}, \end{aligned} \quad (4)$$

where the primes indicate the incident radiation traveling in the substrate and $\mathcal{A}(\mathcal{A}')$ is the intensity absorbed in the film when the radiation is incident on the front (rear) surface. Because of scattering and the finite acceptance angle of the instrument not all of the reflected or transmitted radiation is detected. Equations (4) are modified to read

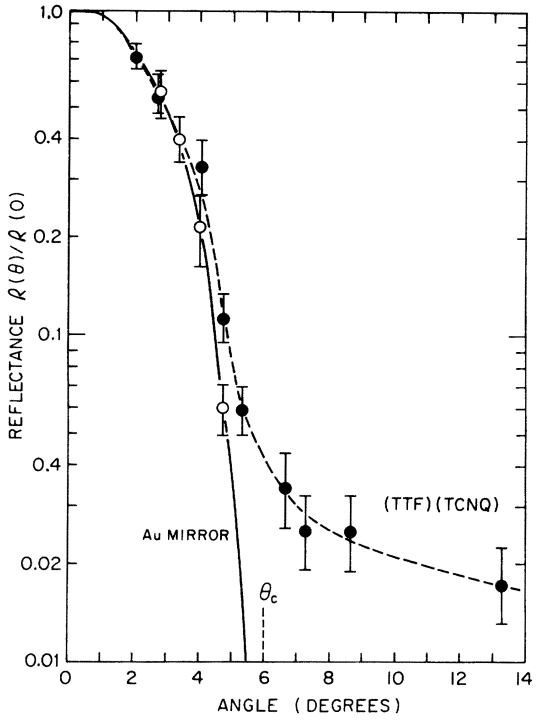

FIG. 16. Reflectance of a TTF-TCNQ film and Au mirror as a function of angle away from the specular reflectance position.

$$\mathcal{T}_{FM}+\mathcal{R}_{FM}+\mathcal{S}_F+\mathcal{A}_F=1 \quad \text{(front)},$$
$$\mathcal{T}_{FM}+\mathcal{R}'_{FM}+\mathcal{S}'_F+\mathcal{A}'_F=1 \quad \text{(rear)}, \tag{5}$$

where $\mathcal{S}_F$ ($\mathcal{S}'_F$) is the intensity scattered, in all directions, when the radiation is incident on the front (rear) film surface. $\mathcal{T}_{FM}$, $\mathcal{R}_{FM}$, and $\mathcal{R}'_{FM}$ are the apparent film coefficients deduced from the measured data. Making the reasonable *ad hoc* assumption that the scattered radiation is proportional to the measured signal, $\mathcal{S}_F=K(\omega)(\mathcal{T}_{FM}+\mathcal{R}_{FM})$ and $\mathcal{S}'_F=K(\omega)(\mathcal{T}_{FM}+\mathcal{R}'_{FM})$, comparison of Eqs. (21) with (22) leads to the conclusion that

$$\mathcal{T}_F=(1+K)\mathcal{T}_{FM},$$
$$\mathcal{R}_F=(1+K)\mathcal{R}_{FM}, \tag{6}$$
$$\mathcal{R}'_F=(1+K)\mathcal{R}'_{FM}.$$

Using the identity

$$\mathcal{R}'_F=n\mathcal{R}_F-(n-1)(1-\mathcal{T}_F), \tag{7}$$

where n is the index of refraction of the substrate, Eqs. (6) can be solved to find

$$K=\frac{(n-1)(1-\mathcal{T}_{FM})-n\mathcal{R}_{FM}+\mathcal{R}'_{FM}}{(n-1)\mathcal{T}_{FM}+n\mathcal{R}_{FM}-\mathcal{R}'_{FM}}. \tag{8}$$

It is thus possible to take three independent sets of data ($\mathcal{T}$, $\mathcal{R}$, and $\mathcal{R}'$) and deduce from them three unknowns [σ_1, $|\epsilon_1-1|$, and $K(\omega)$]. When this is done, the results for $\sigma(\omega)$ at room temperature are shown as the solid line in Fig. 15. This is a much improved result as it closely resembles the single-crystal conductivity. Furthermore, it satisfies the sum rule on the conductivity,

$$\int_0^\infty \sigma_1^b(\omega)\,d\omega=\tfrac{1}{8}\omega_p^2, \tag{9}$$

using a Drude extrapolation above 4000 cm^{-1}.

Figure 17 shows the conductivity of TTF-TCNQ films over the whole frequency range from 20 to 4000 cm^{-1} at four temperatures. The data were obtained from a film grown on KBr (300–4000 cm^{-1}), one on Mylar (100–400 cm^{-1}), and one on sapphire (20–200 cm^{-1}). As the temperature is lowered, the over-all width of the peak is decreased and the height of the peak increased. The inset shows the temperature dependence of the location of the peak in $\sigma_1(\omega)$. This is actually determined from a fit of a Drude-Lorentz expression for the conductivity, as will be discussed below. Note that the minimum in $\sigma_1(\omega)$ centered at 1400 cm^{-1} shows up in the film data as well as the single-crystal data. This minimum becomes shallower and less well-defined at lower temperatures.

As described in our earlier publication,[1] the

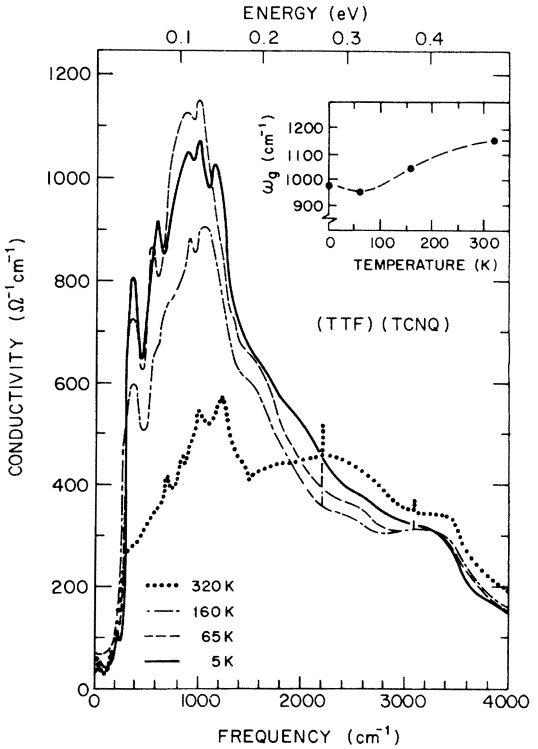

FIG. 17. The real part of the conductivity $\sigma_1(\omega)$ vs frequency at selected temperatures. The inset shows the temperature dependence of the peak in $\sigma_1(\omega)$.

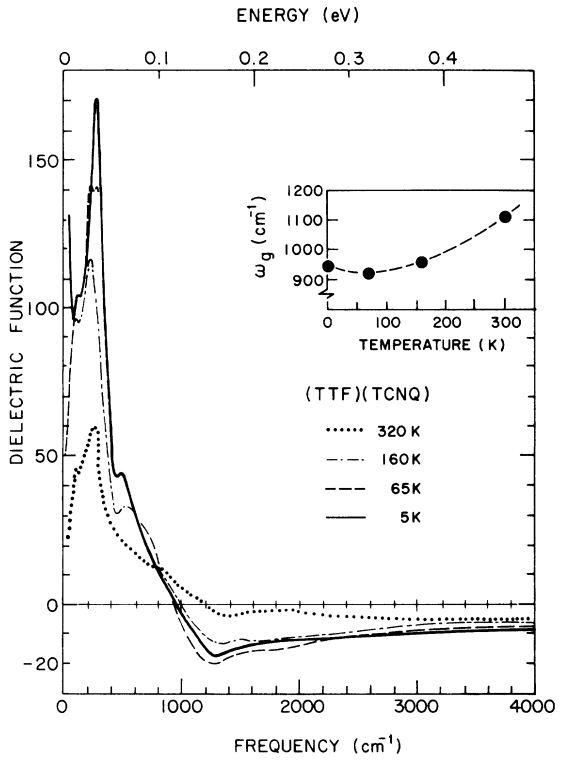

FIG. 18. The dielectric function $\epsilon_1(\omega)$ vs frequency at selected temperatures as determined from Kramers-Kronig transform of the data of Fig. 17. The insert shows the temperature dependence of the crossover frequency where $\epsilon_1 = \epsilon_{core} = 2.4$.

values for $\epsilon_1(\omega)$ determined directly from the film transmission and reflection data and those calculated from a Kramers-Kronig transform of the $\sigma_1(\omega)$ data have the same shape but differ by an almost constant amount (approximately 10) throughout the entire region. The origin of this offset is straightforward. The transverse dielectric constant (below 4000 cm^{-1}) is larger than the core value $\epsilon_{core} = 2.4$, assumed earlier. Figure 9 shows that for these frequencies $\epsilon_1^a \sim 4$. The values for ϵ_1^{c*} appropriate to the c^* direction are not known. However since the c^* conductivity is greater than that along a, one might expect ϵ_1^{c*} to be correspondingly larger. For the films $\epsilon_1^b = 3\langle\epsilon_1\rangle - \epsilon_1^a - \epsilon_1^{c*}$. To obtain agreement with the single-crystal data for ϵ_1^b and the Kramers-Kronig transform of the film conductivity requires $\epsilon_1^{c*} \simeq 10$, a not unreasonable value.

Figure 18 shows the dielectric function $\epsilon_1(\omega)$ at four temperatures as determined from Kramers-Kronig transformation of the data in Fig. 18. The dc and microwave values of the conductivity were used as the low-frequency extrapolation; this ensures that ϵ_1 is large and negative at low frequencies when the temperature is greater than that of the metal-insulator transition. A Drude extrapolation, using the parameters of Bright *et al.*,[12] was used above 400 cm^{-1}. The insert in Fig. 18 shows the frequency at which ϵ_1 crosses $\epsilon_{core} = 2.4$. This is the best definition of the energy gap presently available.

The dielectric function is negative (metallic) at high frequencies, but changes sign between 900 and 1200 cm^{-1} becoming large and positive (like that of a small gap insulator) at low frequencies. In the far infrared $\epsilon_1^b(\omega)$ is decreasing (toward negative values) at temperatures above 60 K, whereas the 5 K data show ϵ_1^b increasing toward the large values observed at microwave frequencies.[7,8]

These TTF-TCNQ films are composed of a large number of small randomly oriented crystallites. The room-temperature dc conductivity of the film falls below $\frac{1}{3}\sigma_1^b(0) \sim 300\ \Omega^{-1}\,cm^{-1}$, but rather is closer to that of a polycrystalline compaction $\sigma_1(0) \sim 6\ \Omega^{-1}\,cm^{-1}$. Thus there is clearly some crossover frequency above which the conductivity derived from the film data corresponds to intrinsic properties of single crystals TTF-TCNQ and below which small-particle effects dominate.

The problem of a composite medium was solved for isotropic spheres in an insulating matrix by Maxwell-Garnett[43] and has been recently discussed by Gentzel and Martin,[44] by Barker,[45] and by Tanner, Sievers, and Buhrman.[46] The theory must be extended to include anisotropy in shape and conductivity and to include the effects of interacting particles. We adopt a simple model system: randomly oriented crystallities such that

$$\langle \vec{E} \cdot \vec{b} \rangle \simeq \tfrac{1}{3} |\vec{E}| , \tag{10}$$

where $\vec{E}$ is the electric field vector and $\vec{b}$ is a unit vector along the crystal axis. The brackets denote an average over all crystallites. We treat the medium as having a volume fraction $\frac{1}{3}f$ (where f is the filling factor of the film) of crystallites with their highly conducting b axes exactly along the electric field. The others have $\vec{E} \perp \vec{b}$ and are taken as part of the matrix in which the highly conducting crystals are suspended. The particles, then, have complex dielectric function ϵ^b and the matrix has dielectric function ϵ_m. The result[42] of the calculation is that the average dielectric function $\langle\epsilon\rangle$ of the medium is given by

$$\langle\epsilon\rangle = \epsilon_m + \frac{\frac{1}{3}f\epsilon_m(\epsilon^b - \epsilon_m)}{\epsilon_m + g(1 - \frac{1}{3}f)(\epsilon^b - \epsilon_m)} , \tag{11}$$

where g is the depolarization factor of the particles. This is found from the solution of the appropriate boundary-value problem and has values between zero (long needle) and unity (slab). The dimensions of the crystallites in these films are typically $3 \times 0.5 \times 0.1\ \mu m^3$. If these are taken as ellipsoid axes, then $g_1 \simeq 0.01$, $g_2 \simeq 0.1$, and $g_3 \simeq 0.9$.

The important term in Eq. (11) is the second one in the denominator. For a conductor, as $\omega \to 0$ the imaginary part of $\epsilon^b \to \infty$ and it dominates the entire expression. In this low-frequency regime, the internal electric field is dominated by depolarization effects.

We set $f \simeq 1$ as appropriate for a film, and the equation is substantially simplified. The dielectric function of the medium is then the transverse dielectric function of TTF-TCNQ $\epsilon_m = \epsilon_\perp$. This will be taken as real and independent of frequency in the far infrared. Taking real and imaginary parts we find

$$\langle \sigma_1 \rangle = \frac{\frac{1}{3}\sigma_1^b}{[1 + (2g\epsilon_1^b/3\epsilon_\perp) - \frac{2}{3}g]^2 + (8\pi g\sigma_1^b/3\omega\epsilon_\perp)^2} , \quad (12)$$

$$\langle \epsilon_1 \rangle = \frac{\frac{1}{3}(\epsilon_1^b + 2\epsilon_\perp) + \frac{4}{3}g(\epsilon_1^b - \epsilon_\perp) + (2g/9\epsilon_\perp)(1+2g)[(\epsilon_1^b - \epsilon_\perp)^2 + (4\pi\sigma_1^b/\omega)^2]}{[1 + (2g\epsilon_1^b/3\epsilon_\perp) - \frac{2}{3}g]^2 + (8\pi g\sigma_1^b/3\omega\epsilon_\perp)^2} . \quad (13)$$

The final term in the denominator of Eqs. (12) and (13) determines the low-frequency response. At high frequencies, where $(8\pi g/3\omega\epsilon_\perp)\sigma_1^b \ll 1$, $\langle\sigma\rangle = \frac{1}{3}\sigma_1^b$. At the lowest frequencies, where $(8\pi g/3\omega\epsilon_\perp)\sigma_1^b \gg 1$, $\langle\sigma\rangle \simeq (3\omega\epsilon_a/8\pi g)^2 (\sigma_1^b)^{-1}$. For the dielectric function at high frequencies, $\langle\epsilon_1\rangle \sim \frac{1}{3}(\epsilon_1^b + 2\epsilon_\perp)$ while at low frequencies, $\langle\epsilon_1\rangle \sim \epsilon_\perp/2g$.

The cutoff frequency below which small-particle effects become important is given by

$$\omega_c = (8\pi g/3\epsilon_\perp)\sigma_1^b . \quad (14)$$

Since $\sigma_1^b(\omega)$ is frequency dependent, ω_c is also. The cutoff frequency is then in effect the highest frequency for which $\omega_c > \omega$. The single-crystal results (Fig. 5) gives $\sigma_1^b(\omega) \simeq 100\ \Omega^{-1}\,\mathrm{cm}^{-1}$ when $\omega = 200\ \mathrm{cm}^{-1}$. From earlier considerations, the transverse dielectric constant is $\epsilon_\perp = \frac{1}{2}(\epsilon_1^a + \epsilon_1^{c*}) \sim 7$. If the highly conducting b axis is the long dimension of the crystallites, then $g = 0.01$ and $\omega_c \sim 6\ \mathrm{cm}^{-1}$. If the crystals are elongated along the a axis, then $\omega_c \sim 60\ \mathrm{cm}^{-1}$.

Interaction among the particles will serve to reduce the cutoff frequency. The particles have a dipole moment $\vec{p} = \Omega\vec{P}_{in} = \Omega(i\sigma/\omega)\vec{E}_{in}$, where $\vec{E}_{in}$ ($\vec{P}_{in}$) is the electric field (polarization) vector inside the particle and Ω is the particle volume. If the field $\vec{E}_{dip}$ from one particle dipole moment is significant at the *surface* of the neighbor, then the particles interact via their polarization, and a polarization current can propogate through the film. Taking r as the mean distance between particle centers, than r^3 is the volume allotted to one particle so that $r = (\Omega/\frac{1}{3}f)^{1/3} \simeq (3\Omega)^{1/3}$. The volume of a particle is $\Omega = \frac{4}{3}\pi x_1 x_2 x_3$, where x_1, x_2, and x_3 are the three semiaxes. In the TTF-TCNQ film the dimensions stand in the proportion $x_1 : x_2 : x_3 = 6 : 1 : 0.2$. Either x_1 or x_2 can be the crystal b axis; x_3 is always the c^* axis. For the purpose of this estimate we take $b = (3\Omega/4\pi)^{1/3}$ (equivalent to taking $ac = b^2$ or $b \sim x_2$). The field from the dipole moment of a particle at the nearest surface of a neighbor at $\vec{r}$ is therefore

$$\vec{E}_{dip} = \left(\frac{1}{\epsilon_\perp}\right)\frac{3(\vec{n}\cdot\vec{E}_{in})\vec{n} - \vec{E}_{in}}{[(3\Omega)^{1/3} - (3\Omega/4\pi)^{1/3}]^3}\,\Omega(i\sigma/\omega) , \quad (15)$$

where $\vec{n}$ is a unit vector along r and $\epsilon_\perp$ is the dielectric constant of the medium surrounding the particle. Taking $\vec{n}$ along $\vec{E}_{in}$ and substituting for the internal field using the standard expression

$$\vec{E}_{in} = \epsilon_m \vec{E}_{ext} / [g\epsilon^b + (1-g)\epsilon_m] ,$$

one finds

$$|E_{dip}| = \frac{1}{\epsilon_\perp}\left(\frac{(\epsilon_1 - 1)^2 + (4\pi\sigma_1/\omega)^2}{[1 + g(\epsilon_1 - \epsilon_\perp/\epsilon_\perp)]^2 + (4\pi g\sigma_1/\omega\epsilon_\perp)^2}\right)^{1/2} |\vec{E}_{ext}| . \quad (16)$$

At high frequencies $\omega \gg 4\pi\sigma$ and $|\epsilon_1| \simeq \epsilon_\perp$, so that $|\vec{E}_{dip}| \simeq |\vec{E}_{ext}|$. As the frequency is reduced $|\vec{E}_{dip}|/|\vec{E}_{ext}|$ increases until at low frequencies,

$$\omega \lesssim (4\pi g/\epsilon_\perp)\sigma_1^b , \quad (17)$$

we have

$$|E_{dip}| \simeq (1/g)|E_{ext}| > |E_{ext}| . \quad (18)$$

Under these circumstances, in zeroth order most of the field at a given particle comes from the polarization of its neighbors thus reducing the surface charge at the particle boundaries. Consequently, small-particle effects are suppressed by interparticle capacitive displacement currents, and the film can be treated as a bulk medium to frequencies below ω_c (note that the dipolar coupling fields become important for $\omega \leq \omega_c$).

Crystals of TTF-TCNQ have been found[7] to grow in two habits; needles elongated along the b axis and needles elongated along the a axis. Consequently it is possible that the thin-film crystallites are mixed, and a range of cutoff values can be expected. Using the theoretical results derived above, we can develop an experimental criteria to determine when small-particle effects become important. There are a number of low-frequency bending fundamentals in the TCNQ molecule, most noticeably the mode at 119 cm^{-1} in TTF-TCNQ. This corresponds to an out of plane bending of the $=C(CN)_2$ wings and is polarized basically along the b axis of the crystal.[47] At this frequency σ_1^b increases. If $\langle\sigma_1\rangle$ also increases, then $\langle\sigma_1\rangle \propto \sigma_1^b$ and

$\omega > \omega_c$. On the other hand, if $\langle\sigma_1\rangle$ decreases then $\langle\sigma_1\rangle \propto [\sigma_1^b]^{-1}$ and $\omega < \omega_c$. As seen in Fig. 14, the line appears as a resonance and not as an antiresonance. Hence ω_c is well below 119 cm^{-1} and probably below 50 cm^{-1} where another resonance line is seen.

Figures 19 and 20 show two examples of the far-infrared conductivity of TTF-TCNQ films, grown on polyethylene and sapphire, respectively, at temperatures both above and below the metal-insulator transition. At low temperatures there is a broad structure centered at 80 cm^{-1}. As the temperature is raised above the metal-insulator transition this structure disappears while the over-all level of the conductivity increases by a factor of two. As the temperature is further increased to 300 K, this level drops by a factor of three (see also Figs. 13 and 14). Notice that the values of $\sigma_1^b(\omega)$ obtained from the film at 300 K are almost identical with those from the single crystal using the Hagen-Reubens low-frequency extrapolation.

Although the two different films have quite similar shapes for $\sigma_1^b(\omega)$, there is a significant difference in the magnitude. This may be partially a consequence of uncertainty in the film thickness and perhaps also of different rates of film growth on different substrates. The film grown on Mylar had numerical conductivity values quite similar to those on polyethylene. The film data reported earlier had lower numerical values than those here, because we were unaware of the radiation leakage problem in the far-infrared reflectance insert. This had almost no effect on the shape of the conductivity-versus-frequency curves but systematically reduced their values. Figure 20, then, shows the corrected data for the sapphire film.

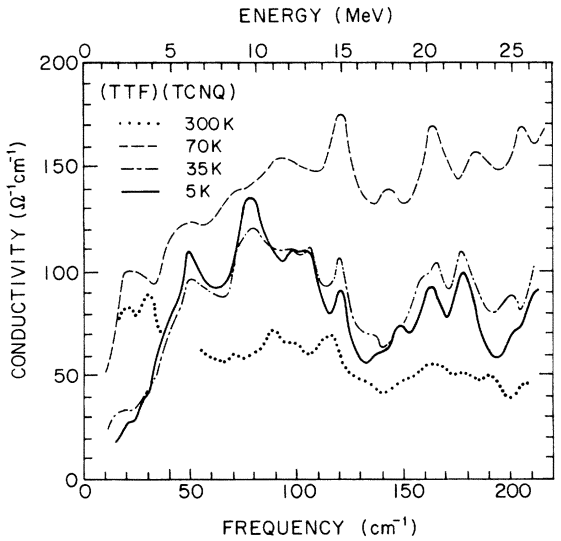

FIG. 19. The frequency dependence of the real part of the conductivity of a thin film grown on polyethylene. Temperatures above and below the metal-insulator transition are shown for the frequency range 20–220 cm^{-1}.

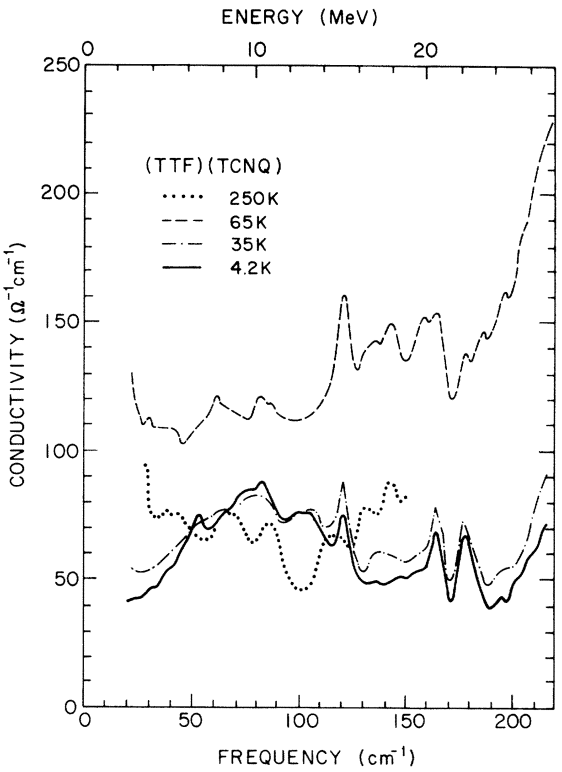

FIG. 20. The frequency dependence of the real part of the conductivity of a thin film grown on sapphire. Temperatures above and below the metal-insulator transition are shown for the frequency range 20–220 cm^{-1}.

Visible on Figs. 19 and 20 are conductivity peaks, most noticeable at 50, 119, 163, and 180 cm^{-1} in the low-temperature data and at 119 and 163 cm^{-1} in the high-temperature data. These are all resonances (increases in conductivity) satisfying the criterion developed above. At 70 K the conductivity of the film grown on polyethylene is falling at frequencies below 50 cm^{-1} suggesting that the small-particle effects are beginning to become important. This is not the case for the film grown on sapphire as shown in Fig. 20. It seems likely that the substrate affects the detailed particle growth so that different substrates will lead to different low-frequency cutoffs.

The existence of molecular resonances and overall reproducibility of the data implies that the thin-film data for $\sigma_1(\omega)$ can be trusted at least out to 50 cm^{-1}. At lower frequencies depolarization effects become increasingly more important. The maximum centered at 80 cm^{-1} at low temperature appears to be an intrinsic feature of the films. However the detailed shape on the low-frequency side may be distorted by small-particle effects.

Transmittance and reflectance measurements were made at lower frequencies (2–30 cm^{-1}) with

a lamellar grating interferometer.[48] The single specimen studied was a rather poor film on Mylar. The conductivities were found to continue to decrease with decreasing frequency; however the conductivity at 4.2 K was always less than that at 70 K. $\sigma_1(2\,\mathrm{cm}^{-1}) \lesssim 1\ \Omega^{-1}\mathrm{cm}^{-1}$ at 4.2 K and $\sigma_1(2\,\mathrm{cm}^{-1}) \sim 20\ \Omega^{-1}\mathrm{cm}^{-1}$ at 70 K. Although small-particle effects are undoubtedly important at the lowest frequencies, it seems that even at 2 cm^{-1} we are not fully into the low-frequency regime where $\langle\sigma\rangle \propto (1/\sigma_1^b)$, i.e., where the denominator in Eq. (12) has completely taken over.

V. GENERAL FEATURES, BAND STRUCTURE, AND OPTICAL MASSES

The properties of TTF-TCNQ in the visible and near-infrared spectral regions were described in earlier publications.[11,12] The measured single-crystal reflectance for $E \parallel b$ showed a plasma edge between 5000 and 7000 cm^{-1} and "metallic" reflectivity at lower frequencies. The results were compared with a Drude-Lorentz expression for $\epsilon(\omega)$,

$$\epsilon(\omega) = \epsilon_1(\omega) + i\epsilon_2(\omega) = \epsilon_{\mathrm{core}} + \omega_p^2/(\omega_g^2 - \omega^2 - i\omega/\tau_{\mathrm{sp}}), \tag{19}$$

or equivalently for the conductivity,

$$\sigma(\omega) = \sigma_1(\omega) + \sigma_2(\omega) = \frac{(\omega_p^2/4\pi)\omega\tau_{\mathrm{sp}}}{\omega - i\tau_{\mathrm{sp}}(\omega^2 - \omega_g^2)} - \frac{i\omega}{4\pi}(\epsilon_{\mathrm{core}} - 1). \tag{20}$$

Here ω_g is the effective energy gap and τ_{sp} is the single-particle relaxation time. The unscreened plasma frequency ω_p is a measure of the oscillator strength since

$$\omega_p^2 = 8\int_0^\infty \sigma_1(\omega)\,d\omega = \frac{\pi}{2}\int_0^\infty \omega\epsilon_2(\omega)\,d\omega. \tag{21}$$

The conclusion of Bright *et al.*[12] was that for the frequencies measured, 5000–10 000 cm^{-1}, the data were accurately described by the conventional Drude expression, implying that $(\omega_g/\omega)^2 \ll 1$ and that τ_{sp} is approximately constant throughout the interval. However, the single-crystal data in Figs. 4, 5, and 8 and the film data in Figs. 17 and 18 clearly show that at lower frequencies there is an energy gap with $\omega_g \simeq 1100\ \mathrm{cm}^{-1}$.

We have interpreted the over-all features of $\sigma_1(\omega)$ for $E \parallel b$ as arising from single-particle excitations across an energy gap. In one-dimensional systems the onset of absorption across a direct gap is described by a joint density of states proportional to $(\omega - \omega_g)^{-1/2}$, so that one can identify ω_g with the frequency of maximum conductivity, i.e., the resonance frequency in the Drude-Lorentz expression. Because $\omega_g\tau_{\mathrm{sp}} \sim 1$, the conductivity is not simply proportional to the joint density of states but must also include the indirect transitions involving multiple phonon processes which give rise to the conventional Drude absorption in metals. We therefore approximate the frequency-dependent conductivity with the Drude-Lorentz expression given in Eqs. (19) and (20). The real part of the conductivity is given by

$$\sigma_1(\omega) = (\omega_p^2/4\pi)\,\omega^2\tau_{\mathrm{sp}}/[\omega^2 + \tau_{\mathrm{sp}}^2(\omega^2 - \omega_g^2)^2], \tag{22}$$

and the real part of the dielectric function by

$$\epsilon_1(\omega) = \epsilon_{\mathrm{core}} + \omega_p^2(\omega_g^2 - \omega^2)/[(\omega_g^2 - \omega^2)^2 + \omega^2/\tau_{\mathrm{sp}}^2]. \tag{23}$$

Notice that when $\omega = \omega_g$, $\sigma_1(\omega) = \omega_p^2\tau_{\mathrm{sp}}/4\pi$ (its maximum value), while $\epsilon_1(\omega_g) = \epsilon_{\mathrm{core}}$. The fit to the room-temperature single-crystal data is shown as the dashed lines on Figs. 21 and 22 using $\omega_p = 9560\ \mathrm{cm}^{-1}$ and $\epsilon_{\mathrm{core}} = 2.4$. The resulting fit yields $\omega_g = 1100\ \mathrm{cm}^{-1}$ and $\tau_{\mathrm{sp}} = 3.1 \times 10^{-15}$ sec. The value of τ_{sp} is consistent with that obtained earlier from single-crystal experiments near the plasma edge.[12] The corresponding fits to the film data are shown in Fig. 23 as the solid lines, again using $\omega_p = 9560\ \mathrm{cm}^{-1}$. The calculated curve was obtained by adding to the conductivity in Eq. (41) a small constant conductivity $\sigma_m = 60\ \Omega^{-1}\mathrm{cm}^{-1}$. This gives a small but noticeable improvement to the fit. The room-temperature parameters are found to be $\omega_g = 1150\ \mathrm{cm}^{-1}$, in excellent agreement with the single-

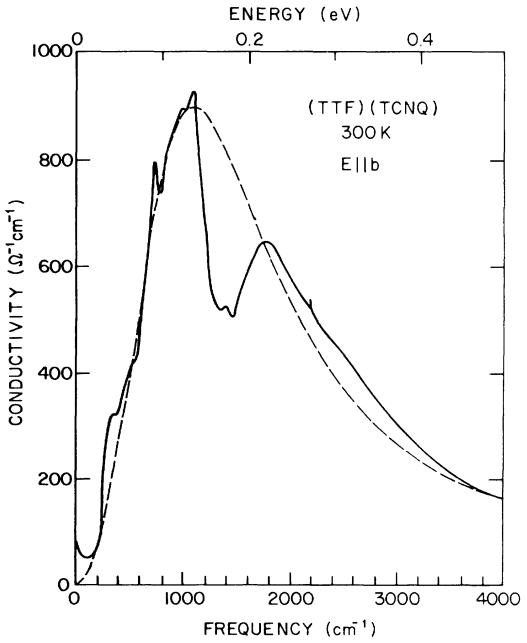

FIG. 21. Fit of the Drude-Lorentz model [Eq. (22)] to the real part of the conductivity of TTF-TCNQ for a single crystal with $E \parallel b$, over the frequency range 100–4 000 cm^{-1}. The parameters are listed in Table I.

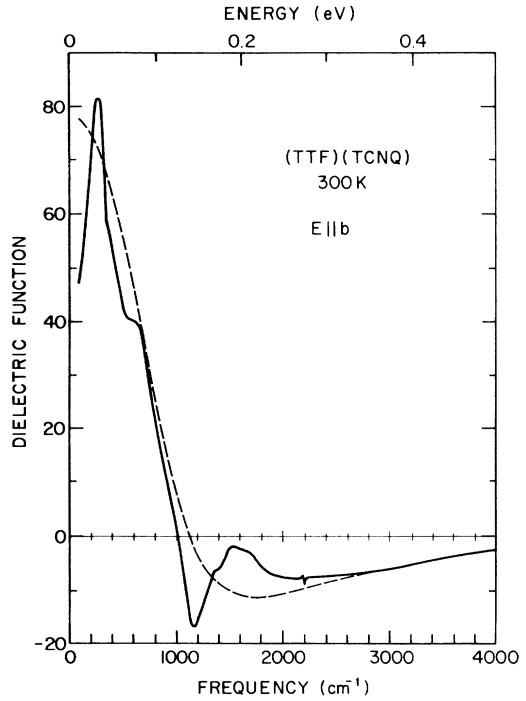

FIG. 22. Fit of the Drude-Lorentz model [Eq. (23)] to the real part of the dielectric function of TTF-TCNQ for a single crystal with $E \| b$ over the frequency range 100–4 000 cm^{-1}. The parameters are listed in Table I.

crystal data, and $\tau_{sp} = 1.8 \times 10^{-15}$ sec^{-1}, somewhat shorter as might be expected from surface scattering and chain defects. Table I summarizes the parameters for all the calculated curves.

The Drude-Lorentz model given by Eqs. (19) and (20) is expected to provide an adequate description of the over-all features of the small band-gap *one-dimensional* semiconductor because of the singularity in the density of states at the band edge. We have also obtained excellent fits to the single-crystal reflectivity data for KTCNQ[49] and to $\sigma_1(\omega)$ and $\epsilon_1(\omega)$ for the one-dimensional conductor $K_2Pt(CN)_4Br_{0.3} \cdot 3H_2O$(KCP).[50]

At frequencies below the onset of interband transitions (i.e., $< 10^4$ cm^{-1}), we expect the over-all oscillator strength to be associated with a single relatively narrow energy band with a small band gap at the Fermi surface owing to the Peierls's effect. The near-ir single-crystal reflectivity data were analyzed by writing the measured plasma frequency in the conventional form

$$\omega_p^2 = 4\pi N e^2/m^* , \tag{24}$$

where N is the density of electrons in the band, and m^* is the optical effective mass calculated in a tight-binding model.

Additional information can be extracted from the oscillator strength using the sum rule. The effective number of electrons per unit cell participating in optical transitions for energies less than $\hbar\omega$ is given by

$$\frac{m}{m^*} N_{eff}(\omega) = \left(\frac{1}{8}\int_0^{\omega} \sigma_1(\omega^1)\, d\omega^1\right) \Big/ \frac{4\pi N_c e^2}{m} , \tag{25}$$

where N_c is the number of unit cells per unit volume. $N_c = 4.7 \times 10^{21}$ cm^{-1} for TTF-TCNQ. The result of this calculation is shown in Fig. 24. $N_{eff}(\omega)$ has a gentle plateau just below the onset of interband transitions at about 10^4 cm^{-1}. The extrapolated saturation value (i.e., associated with the solid-state region below the interband edge) is

$$N_{eff}\, m/m^* \cong 0.2 . \tag{26}$$

This value is in excellent agreement with previous estimates based on the oscillator strength as obtained from the plasma frequency. Assuming nearly complete change transfer, $N_{eff} \sim 1$ and $m^* = 5m_e$. If N_{eff} is less than unity (incomplete charge transfer), m^* must be correspondingly reduced. Since the low-temperature x-ray measurements[17] show that $N_{eff} \simeq 0.6$ we conclude that the optical mass is approximately $3m_e$.

Above 10^4 cm^{-1}, $N_{eff}(\omega)$ rises steeply due to what are presumably excitonic and interband tran-

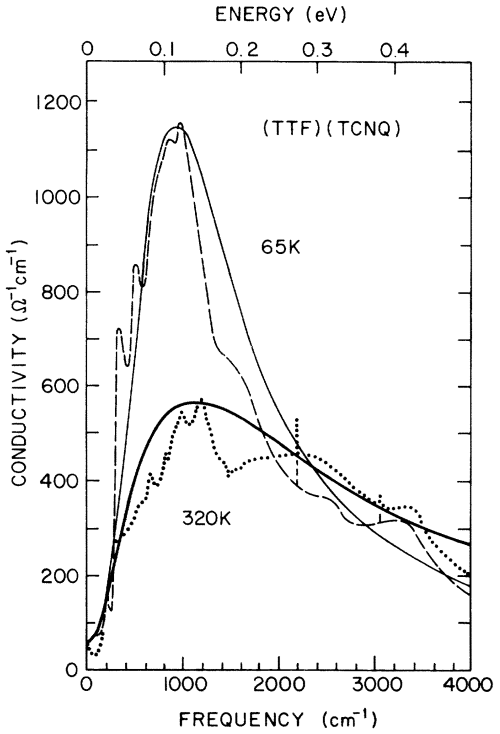

FIG. 23. Fit of the Drude-Lorentz model [Eq. (22)] to the real part of the conductivity of TTF-TCNQ, derived from film data, at 320 and 65 K, over the frequency range 20–4 000 cm^{-1}. The parameters are listed in Table I.

TABLE I. Drude-Lorentz parameters.

	Temperature (K)	ω_g (cm^{-1})	τ_{sp} (sec)	$1/\tau_{sp}$ (cm^{-1})	ω_g (cm^{-1})	ϵ_{core}
TTF-TCNQ single crystal	300	1100	3.1×10^{-15}	1640	9560	2.4
TTF-TCNQ film	320	1150	1.8×10^{-15}	2800	9560	2.4
TTF-TCNQ film	160	1040	3.4×10^{-15}	1450	9560	2.4
TTF-TCNQ film	65	950	3.8×10^{-15}	1300	9560	2.4
TTF-TCNQ film	5	980	3.8×10^{-15}	1300	9560	2.4

sitions. No attempt has been made to identify the structure in σ_1^b at these high frequencies.

The plasma edge in the single-crystal reflectance spectra indicates a well defined longitudinal excitation, interpreted as a volume plasmon. This is confirmed by the loss function $\mathrm{Im}(1/\epsilon)$ shown in Fig. 25. This function has resonances at frequencies corresponding to electromagnetically coupled longitudinal oscillations which could be excited by (for example) charged particles. Hence the loss function is essentially proportional to the energy-loss spectrum of fast electrons traversing a solid sample in the b direction. The plasmon line is seen to be quite sharp with a half width of 1600 cm^{-1} and plasmon energy of 6100 cm^{-1} (0.756 eV) in agreement with the value inferred from Bright *et al.*,[11,12] $\omega_p/\epsilon_{core}^{1/2} = 6120$ cm^{-1}. The structure at higher frequencies is again due to interband transitions. A weaker line is seen at 2.8×10^4 cm^{-1}.

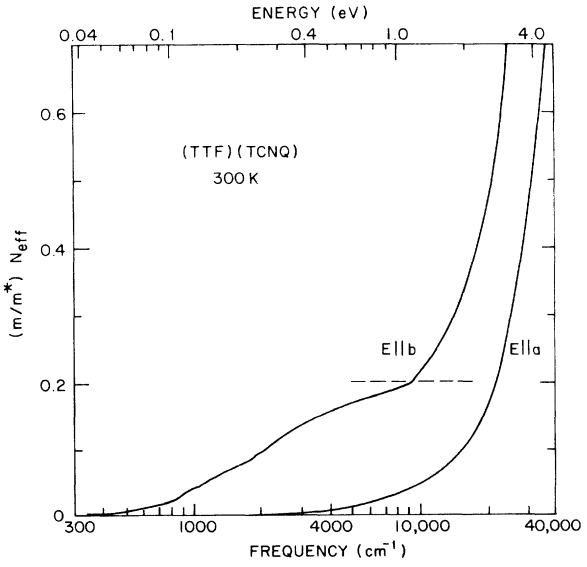

FIG. 24. Number of effective electrons, obtained from the oscillator strength sum rule, for TTF-TCNQ for two polarizations, vs frequency from 300 to 37 000 cm^{-1}. Notice the logarithmic frequency scale. The gentle plateau for $E \| b$ implies the exhaustion of the single tight-binding band oscillator strength just below the onset of interband transitions.

The loss function shown in Fig. 25 has been studied directly by Ritsko *et al.*[51] via electron energy-loss experiments (inelastic electron scattering) from oriented films of TTF-TCNQ. The observed loss function is in excellent agreement with that presented here over the region of energy overlap. The frequencies, widths, and intensities of the loss peaks are nearly identical to those shown in Fig. 25. The detailed agreement gives additional confidence in the optical constants as derived from the reflectivity data by the Kramers-Kronig analysis.

Optical properties for $E \| a$. At dc and microwave frequencies the transverse conductivity is small $\sigma_a \sim 1$ $(\Omega\,\mathrm{cm})^{-1}$ at room temperature.[4,7] The magnitude and temperature dependence of σ_a was explained by diffusive transport caused by the thermal disorder in the lattice at finite temperatures.

This conclusion is entirely consistent with the a-axis optical data as shown in Figs. 5, 6, 8, 10, and 11. There is no observable a-axis plasma

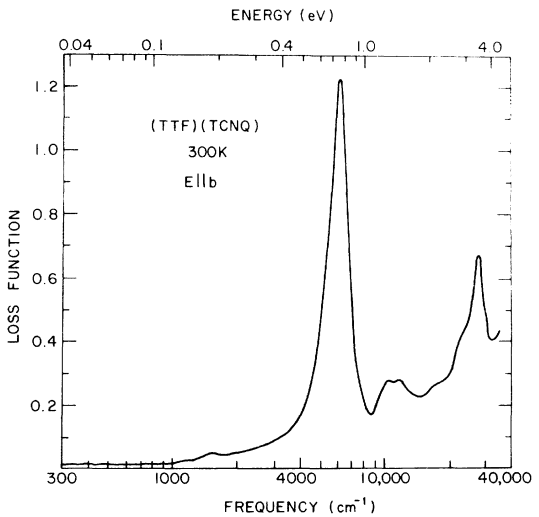

FIG. 25. Loss function $\mathrm{Im}(1/\epsilon)$ of TTF-TCNQ, obtained from the optical constants for $E \| b$, vs frequency from 300 to 37 000 cm^{-1}. Notice the logarithmic frequency scale. The results are in excellent agreement with the electron energy-loss measurements of Ritsko *et al.* (Ref. 51).

frequency; $\epsilon_1^a(\omega)$ never crosses zero. This is as expected for such an anisotropic system where $\omega_p^a \ll \omega_p^b$ since the transverse effective mass is extremely large. Consequently $(\omega_p^a)^2\tau^2 \ll 1$ and the transverse plasma oscillations are overdamped. In effect, band theory is not appropriate and a diffusive transport theory is implied.

Application of the sum rule to $\sigma_1^a(\omega)$ is presented in Fig. 24. No plateau of any kind is observed. Basically $(m/m_a^*)N_{\text{eff}}(\omega)$ remains small throughout the solid state region ($\omega < 5000$ cm^{-1}) and then increases sharply at the onset of interband transitions.

The a-axis dielectric function is shown in Fig. 11. Above 300 cm^{-1}, $\epsilon_1^a(\omega)$ varies slowly and increases with decreasing frequency with the expected steps associated with intramolecular bond-vibration resonances clearly visible. The value obtained for ϵ_1^a at 300 cm^{-1} is approximately 4.5, considerably below the value of 30 obtained at microwave frequency (10^{10} Hz) at room temperature. The excess low-frequency dielectric constant must arise from additional structure in $\sigma_1^a(\omega)$ at long wavelengths.

The magnitude of $\sigma_1^a(\omega)$ at 300 cm^{-1} is about 2 $(\Omega\ \text{cm})^{-1}$; i.e., comparable to that found at dc and microwave frequencies. The observed frequency dependence of $\sigma_1^a(\omega)$ in the interval below 5000 cm^{-1} is interesting in the context of studying diffusive transport in thermally disordered solids. A detailed theoretical analysis in this regime is not presently available.

VI. ENERGY GAP AND PINNED MODE

The experimental results presented in Secs. III and IV of this paper are consistent with the model described in Sec. I, that of a Peierls-Fröhlich giant density-wave conductor. In this section these results will be analyzed in the context of this model. The existence of an energy gap in the excitation spectrum of TTF-TCNQ is a principal result of this paper. TTF-TCNQ is not a simple metal. It has the optical properties of a semiconductor but conducts at dc ($T > 58$ K) due to a narrow peak in $\sigma_1(\omega)$ centered at zero frequency, which we call the collective mode. Using the mean-field result[52] connecting the gap energy ($\hbar\omega_g = 0.14$ eV) and the characteristic temperature T_ρ, one obtains

$$T_\rho = \hbar\omega_g/3.5\,k_B \simeq 430\ \text{K}, \tag{27}$$

well above room temperature. This is consistent with the presence of a gap in the energy spectrum at all temperatures (see Figs. 3 and 15).

A high mean-field temperature for TTF-TCNQ was suggested by Lee, Rice, and Anderson[53] in order to explain the temperature dependence of the magnetic susceptibility. The susceptibility is a measure of the density of states at the Fermi level and, in TTF-TCNQ, increases considerably on going from 60 to 300 K.[14] This was explained[53] as arising from fluctuation effects below the mean-field temperature. Fluctuations are known to be important in 1D systems and allow for states in the gap for $T < T_\rho$, so that the theoretical density of states does not have a well-defined energy gap until temperatures well below T_ρ.

The infrared conductivity however does show a distinct energy gap even at room temperature. We conclude that the gap in $\sigma_1(\omega)$ is in essence a mobility gap caused by the strong dynamic fluctuations in local potential due to the inherent fluctuations in the one-dimensional Peierls-Fröhlich state below the mean-field temperature. The existence of a mobility gap in KCP has been noted by Zeller[54] and by Brüesch *et al.*[50] Below the three-dimensional ordering temperature, the ordered state would be expected to lead to a true semiconducting gap, and indeed the residual background conductivity in the gap region below 200 cm^{-1} decreases significantly compared with that at 70 K (see Figs. 14, 19, and 20).

The over-all temperature dependence seen between 200 and 10 000 cm^{-1} is mainly a sharpening of the whole structure with decreasing temperature (Figs. 17 and 18). In agreement with the near-ir studies,[11,12] the relaxation time τ_{sp} changes by approximately a factor of two with most of the change taking place between 320 and 70 K. This sharpening may be due to the vanishing of the phonon absorption term in $\tau_{sp}(\omega)$ and perhaps also in part due to the above mentioned fluctuation effects.

In addition to the sharpening of the spectrum, a small nonmonotonic shift of the gap position is observed as indicated by the position of the conductivity maximum (see Fig. 17) and by the zero crossing of the dielectric function (see Fig. 18). The behavior is similar to that of the maximum in the Lee, Rice, and Anderson[53] fluctuation density of states although no quantitative comparison can be made.

The far-infrared reflectivity studies (beyond 50 cm^{-1}) are incomplete in that single-crystal data are not yet available. Such experiments must await the existence of large single crystals. However, the measurements on thin-film samples demonstrate the important features, seen in Figs. 13, 14, 19, and 20. As the temperature is decreased from room temperature, the average value of the far-infrared conductivity first rises by a factor of three and then, below the 58-K metal-insulator transition, falls by a factor of two at low temperatures. Below 58 K a broad resonant structure appears, centered at 80 cm^{-1}. Its strength grows rapidly between 58 and 40 K and remains relatively unchanged below 40 K.

The temperature dependence of the average val-

ue of the conductivity in the far ir must be understood in the context of a high-temperature metallic state with a metal-insulator transition at 54 K. The 54-K transition is a three-dimensional ordering of the TTF-TCNQ system as evidenced by thermodynamic studies which show a phase transition with structure in the specific heat[16] and spin susceptibility.[14] Below this temperature, the dc[3-6] and microwave[7,9,10] conductivities fall dramatically.

The increase in far-ir conductivity with decreasing temperature is consistent with the two-chain model developed in connection with the magnetic susceptibility.[14] The metallic chain would be expected to show an increasing conductivity as the temperature is lowered; then below the three-dimensional ordering temperature, to fall to a small value. The absolute value in the gap region (Figs. 19 and 20), although small, is of order 100 $\Omega^{-1}\,\mathrm{cm}^{-1}$ which is comparable to conductivities in other conducting TCNQ salts.

Alternatively, the residual conductivity may be that of the other two directions, in which case it must be mostly due to σ_1^{c*}, since below 300 cm^{-1} $\sigma_1^a < 3\ \Omega^{-1}\,\mathrm{cm}^{-1}$ at room temperature (Fig. 10). This would require $\sigma_{1(\omega)}^{c*} \sim 40\ \Omega^{-1}\,\mathrm{cm}^{-1}$ in the far-ir. As the temperature is reduced this would rise as does the dc conductivity. At the three-dimensional ordering temperature, the energy gap is established in all directions and the conductivity will fall accordingly.

A variety of measurements suggest the existence of an activation energy Δ in the low-temperature phase with magnitude of order $\Delta \simeq 80$ K. dc conductivity,[3-6] microwave conductivity,[7] and electron-spin susceptibility[14] all yield values of this order. However, the optical data show no sign of the large oscillator strength expected for a direct electronic transition at frequencies below 200 cm^{-1}. Moreover, the energy gap ($\omega_g \sim 1050\ \mathrm{cm}^{-1}$) observed in the metallic regime persists into the low-temperature phase. The only significant change is the disappearance of the collective mode near $\omega = 0$ and the associated appearance of the large dielectric constant due to the pinned mode. Evidently, the smaller activation energy indicated by $\chi(T)$ has little or zero optical oscillator strength.

In a previous publication, we interpreted the low-temperature 80 cm^{-1} resonance as the pinned mode associated with the collective state.[1] According to Lee, Rice, and Anderson,[21] a collective mode which carries a finite amplitude charge-density wave will be pinned below the three-dimensional ordering temperature leading to a metal-insulator transition at which the collective-mode contribution to σ_1 will shift away from zero frequency to a characteristic pinning frequency ω_T. A pinned Fröhlich mode has apparently been observed in KCP in the far ir by Brüesch and Zeller.[50,55]

Additional evidence of the pinned mode is obtained from microwave studies of TTF-TCNQ at low temperatures.[7,8,10] Values of the conductivity and dielectric constant along different crystallographic axes were determined using the cavity perturbation method of Buravov and Shchegolev[56] on crystals having normal or transverse crystallographic habits. The results at the lowest temperature ($T = 4.2$ K) show[7,10] the microwave conductivity along the principal conducting b axis exceeds the dc values by three orders of magnitude [$\sigma_1^b(4.2\ \mathrm{K}) \simeq 1\ \Omega^{-1}\,\mathrm{cm}^{-1}$] and the real part of the dielectric constant is unusally large [$\epsilon_1^b(4.2\ \mathrm{K}) = (3.2 \pm 0.7) \times 10^3$]. In contrast, the dielectric constant in the transverse a direction was found to be $\epsilon_1^a(4.2\ \mathrm{K}) = 6 \pm 2$. The large value for ϵ_1^b and the dielectric anisotropy have recently been confirmed with dielectric resonator techniques.[8]

Both σ_1^b and ϵ_1^b can be understood in terms of the pinned mode. The low-temperature microwave results showing the conductivity exceeding the dc values by three orders of magnitude are interpreted as arising from the tail of the 80 cm^{-1} broad maximum. The low-frequency dielectric function of the pinned Fröhlich state contains two contributions, a single-particle contribution (proportional to ω_p^2/ω_g^2) and a collective-mode contribution. The infrared optical studies indicate that more than 99% of the single-particle oscillator strength lies at frequencies above 150 cm^{-1}, contributing less than 100 to ϵ_1^b (4.2 K). Thus the major contribution to ϵ_1^b (4.2 K) is associated with the pinned mode. Note that in Fig. 18, the data in the metallic regime (320, 160, and 65 K) all show $\epsilon_1^b(\omega)$ decreasing toward zero in the far ir; whereas at 5 K, $\epsilon_1^b(\omega)$ increases in the far ir toward the large microwave value. Estimates of $\epsilon_1^b(\omega)$ from a Kramers-Kronig integral, calculated by extrapolating the far-infrared conductivity through the value for the 10-GHz microwave conductivity $\sigma_1^b = 0.5\ \mathrm{cm}^{-1}$, yield a pinned-mode contribution of $(0.5-1) \times 10^3$. The width and central frequency of the pinned mode are expected to be sensitive to defect and surface pinning mechanisms which would be largest in thin films. The low-temperature dielectric constant (ϵ_1^b) was found to increase in magnitude with increasing sample purity,[7] a result also noted recently for the electronically one-dimensional salt KCP.[51] The effect of trace amounts of nonspecific impurities in TTF-TCNQ is to decrease the low-temperature value of ϵ_1^b from approximately 3×10^3 to $(0.5-1) \times 10^3$ while simultaneously diminishing the excess microwave conductivity characteristic of known pure samples. Both of these effects are consistent with increased pinning at low temperatures due to impurities and surface effects. Single-crystal

polarized far-ir transmission and reflection experiments are in progress in our laboratory.[58] The results imply a shift of the pinned mode in single crystals to lower frequencies as expected. Single-crystal direct-absorption measurements (apparently unpolarized) imply a pinning frequency of approximately[37] 7 cm^{-1}.

The temperature dependence of the pinned mode, as illustrated in Fig. 14, is unusual. There is no shift whatever in the center frequency, but rather the strength of the mode goes away rapidly between 40 and 60 K. This is just opposite to expectations based on straightforward considerations in which one might argue that the pinning frequency would go soft as the temperature is raised towards T_{3D}, with the oscillator strength remaining approximately constant. Allender, Bray, and Bardeen[26] have shown that N_F, the number of carriers per unit volume participating in the collective mode, is given by $N_F \simeq N\Delta^2(T)/\Delta^2(0)$ where $\Delta(T)$ is the order parameter of the Peierls-Fröhlich state. It has the BCS or mean-field temperature dependence[52] with characteristic temperature T_p ~ 430 K. N_F should therefore be roughly temperature independent below 200 K and, as a result, so should the collective-mode oscillator strength given by

$$\Omega_p^2 = 4\pi N_F e^2/M^* = 8\int_0^\infty \sigma_{1F}(\omega)\,d\omega\,, \tag{28}$$

where M^* is the effective mass of the coupled electron-lattice mode and σ_{1F} the collective-mode contribution to the conductivity.

The oscillator strength in the pinned mode (normalized to the low-temperature value) as a function of temperature is shown in Fig. 26. To find Ω_p^2 it is necessary to separate the contribution to the conductivity of the pinned collective mode from that of other sources. We have taken the zero to be somewhat below the minimum conductivity between 130 and 200 cm^{-1}. At 4.2 K this is at $\sigma = 40\ \Omega^{-1}\ cm^{-1}$ for the film grown on polyethylene and at $\sigma = 25\ \Omega^{-1} cm^{-1}$ for the film grown on sapphire. At higher temperatures the zero level increases. Figure 26 demonstrates that the oscillator strength of the pinned mode is not constant below $T_{3D} \simeq 58$ K. We conclude that the contribution that is disappearing from the pinned mode is reappearing in the collective mode at zero frequency. As the temperature is raised toward T_{3D} fluctuations and/or thermal excitations act to depin portions of the chain, leaving them free to slide for some time before being repinned. If ψ is the order parameter describing the three-dimensional ordering, the oscillator strength in the pinned mode will go as ψ^2.

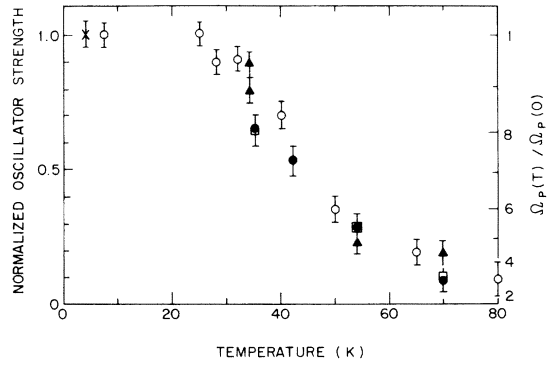

FIG. 26. Oscillator strength in the pinned mode seen in TTF-TCNQ films vs temperature from 4.2 to 70 K. Full circles, film on sapphire; open circles, second film on sapphire; triangles, film on polyethelene; rectangles, film on Mylar.

The temperature dependence below T_{3D} of the dc and microwave conductivities and of the microwave dielectric constant can be understood in terms of this depinning of regions along the chains. The dc[59] and microwave conductivities[60] show a change of slope between 35 and 40 K, rising more steeply above these temperatures. The values of the dc conductivity at 43 and 300 K are numerically equal. This is consistent with an increasing fraction of high-conductivity regions above these temperatures.

The structural data[17] are in agreement with these observations. Between 38 and 54 K, the superlattice peaks shift and broaden toward the diffuse 1 D scattering characteristic of $T > 54$ K. As the superlattice Bragg peaks disappear the pinned-mode oscillator strength shifts to zero frequency.

If some portion of a chain is highly conducting (with the collective mode at zero frequency), the polarizability and, hence, the dielectric constant of the chain will increase. Overscreening in the metallic sense (leading to large negative dielectric constants) is prevented by both the finite lifetime and finite spatial extent of the high-conductivity chains. This physical situation can be treated using an effective-medium theory. A volume fraction f of the material contains unpinned chains, viewed as long ellipsoids lying along the b axis. The ellipsoids have depolarization factor g and (complex) dielectric function $\epsilon(\omega) = 1 - \Omega_p^2/(\omega^2 + i\omega/\tau_c)$ characteristic of a metal. The remainder of the material, occupying volume fraction $(1-f) = \psi^2(T)/\psi^2(0)$, contains pinned chains with dielectric constant ϵ_m. Then, using Eq. (11) we find immediately that the low-temperature (complex) dielectric function is given by

$$\epsilon^b(\omega) = \epsilon_m + \frac{f[\Omega_p^2 + \epsilon_m(\omega^2 + i\omega/\tau_c)]}{[\Omega_p^2 g(1-f)/\epsilon_m] - [1 - g(1-f)](\omega^2 + i\omega/\tau_c)}\,, \tag{29}$$

where we have used $\epsilon_m > 2\omega_p^2/3\omega_g^2 \gg 1$. Except for the second term in the numerator this is a Lorentzian oscillator of strength $f\Omega_p^2/[1-g(1-f)]$ and resonant frequency

$$\omega_0 = \Omega_p\{g(1-f)/[\epsilon_m - \epsilon_m g(1-f)]\}^{1/2} . \quad (30)$$

The second term in the numerator of Eq. (29) is only important for frequencies $\omega > \Omega_p/\epsilon_m^{1/2} > \omega_0$. At zero frequency the real part becomes, taking $\epsilon_m = \epsilon_1^b(0, 0)$ (the microwave dielectric constant 4.2 K),

$$\epsilon_1^b(0, T)/\epsilon_1^b(0, 0) = 1 + f(T)/g[1-f(T)]. \quad (31)$$

As the temperature is raised, $f(T)$ increases, $1-f$ decreases, and g decreases (the depinned regions get longer and longer). The result can be an increasing or decreasing $\epsilon_1^b(0, T)$ depending on whether g or f is the stronger function of T. We conclude from the far-ir and microwave studies that for TTF-TCNQ the depinning commences near 40 K coming to completion near 58 K where the dc conductivity is maximum.

The collective-mode lifetime τ_c has not yet been measured directly but it can be estimated from the measured dc conductivity and the collective-mode oscillator strength Ω_p^2, since

$$\sigma_F = (1/4\pi)\Omega_p^2 \tau_c. \quad (32)$$

An *upper* limit to Ω_p can be estimated from the single-crystal data. Assuming $1/\tau_c$ is less than the lowest measuring frequency, we can write $\epsilon_1 \sim 100 - \Omega_p^2/\omega^2$. There should be a local minimum in $\Re(E \parallel b)$ when $\epsilon_1 = 0$ (at $\omega_{L0} = \Omega_p/10$) with a rapid rise toward $\Re(E \parallel b) = 1$ at lower frequency. This does not happen above 50 cm^{-1}, so we can conservatively construct the inequality $\Omega_p < 1000$ cm^{-1}. Since $\sigma_{dc}^b(300\text{ K}) \sim 10^3$ $(\Omega\,cm)^{-1}$, $\tau_c^{-1} < 3\times10^{12}$ sec^{-1} (16 cm^{-1}). Assuming an increase of oscillator strength of less than a factor of 2 in cooling to 58 K where the peak conductivity is between 10^4–10^5 $(\Omega\,cm)^{-1}$ yields the result $\tau_c^{-1} < 10^{11}$ sec^{-1} (0.5 cm^{-1}). The collective-mode lifetime is enhanced over the single-particle scattering time by at least two orders of magnitude at room temperature and more than three orders of magnitude near 60 K. This comparison represents one of the clearest indications of coherence in the "metallic" state of TTF-TCNQ.

The strength of the collective mode can also be estimated from the 4.2 K thin-film data seen in Figs. 19 and 20. The temperature dependence has been discussed above (Fig. 26). At 4.2 K, $\Omega_p \simeq 400$ cm^{-1}.

Using the definition

$$\Omega_p^2 = 4\pi N_F e^2/M^* = \omega_p^2 m^*/M^* , \quad (33)$$

we estimate $M^* \simeq 600m^*$. Allender, Bray, and Bardeen[26] have found an expression for the effective mass of the collective mode

$$\frac{M^*}{m^*} = \frac{16\pi^2}{7\xi(3)}\left(\frac{kT_p}{\hbar\omega_{2k_F}}\right)^2 \frac{1}{\lambda} , \quad (34)$$

where λ is the dimensionless electron-phonon coupling constant and $\hbar\omega_{2k_F}$ is the energy of the $2k_F$ phonon which drives the Peierls distortion. Lee, Rice, and Anderson[21] obtained an essentially similar expression

$$M^*/m^* = 1 + (E_g/\hbar\omega_{2k_F})^2/\lambda , \quad (35)$$

which differs only by a numerical factor. Craven *et al.*[16] have shown that, if the Peierls distortion does not affect the bandwidth of the high-temperature metallic state,

$$E_g = (8/e)E_F e^{-1/\lambda} . \quad (36)$$

Using the generally agreed upon[12,61] value of $E_F \sim 0.2$ eV (1600 cm^{-1}) and $E_g = 0.14$ eV, we obtain $\lambda = 0.7$. Then, from either (34) or (35), using $\omega_{2k_F} = 50$ cm^{-1} (a little below ω_D), one obtains $M^* = 800m^*$ near the experimentally determined value. The value of λ is of order unity in general agreement with the value obtained by Bright *et al.*[12] from the temperature dependence of the optical scattering time $\tau_{sp}(T)$. Given the uncertainty of the various parameters, the over-all numerical consistency is satisfactory.[58]

VII. DEVIATIONS FROM DRUDE-LORENTZ BEHAVIOR

In this section we discuss the deviations from the Drude-Lorentz form in the single-particle spectral range above the gap; i.e., $\omega > 10^3$ cm^{-1}. The dominant feature is the relatively sharp minimum in $\sigma_1(\omega)$ seen in both the single-crystal data and the film data in the vicinity of 1400 cm^{-1}. This resonant structure suggests either a corresponding resonance in the complex relaxation rate $\Gamma(\omega)$ or a frequency-dependent complex gap function. The possibility of the secondary maximum arising from band-structure effects (e.g., two gaps corresponding to a two-chain model) can be ruled out by noting that such structure would sharpen at low temperatures. In contrast, the data of Figs. 13 and 17 show the strongest effects at room temperature with no sharpening evident.

Gutfreund, Horowitz, and Weger[62] assumed that the structure had its origin in $\tau_{(\omega)}^{-1}$, associated with resonant scattering of the electrons by $2k_F$ optical phonons, arising from the C≡N molecular vibrations. Such a frequency dependence can be incorporated into a generalized Drude-Lorentz expression,

$$\sigma^b(\omega) = \frac{(\omega_p^2/4\pi)\omega}{\omega\Gamma(\omega) - i(\omega^2 - \omega_g^2)} - \frac{i\omega}{4\pi}(\epsilon_{core} - 1) , \quad (37)$$

where $\Gamma(\omega) = \Gamma_1(\omega) + i\Gamma_2(\omega)$ is the complex relaxation rate. Solving for the real and imaginary parts, $\Gamma_1(\omega)$ and $\Gamma_2(\omega)$, in terms of the measured complex dielectric function, one obtains

$$\Gamma_1(\omega) = \frac{4\pi\omega_p^2\sigma_1^b(\omega)}{\omega^2[\epsilon_1^b(\omega) - \epsilon_{\text{core}}]^2 + 16\pi^2[\sigma_1^b(\omega)]^2}, \tag{38}$$

$$\Gamma_2(\omega) = \frac{\omega_p^2\omega[\epsilon_1^b(\omega) - \epsilon_{\text{core}}]}{\omega^2[\epsilon_1^b(\omega) - \epsilon_{\text{core}}]^2 + 16\pi^2[\sigma_1^b(\omega)]^2} + \frac{\omega^2 - \omega_g^2}{\omega}. \tag{39}$$

Note that $\Gamma_1(\omega)$ is completely determined by the experimental data and the two parameters ω_p^2 and ϵ_{core}. $\Gamma_2(\omega)$ involves the additional parameter ω_g. Using the experimentally determined dielectric function as obtained from the single-crystal data of Fig. 3, we have determined $\Gamma_1(\omega)$ and $\Gamma_2(\omega)$ as shown in Fig. 27, using the values $\omega_p = 9560\ \text{cm}^{-1}$, $\epsilon_{\text{core}} = 2.4$, and $\omega_g = 1150\ \text{cm}^{-1}$. The arrows at 6000 cm^{-1} on Γ_1 indicate the range of values in $1/\tau$ found at room temperature by Bright *et al.*[12]

The mechanism proposed by Gutfreund *et al.*[62] is the direct analogue of the Holstein process of phonon emission effects on the far-ir conductivity of metals. This process was first described by Holstein[63] and observed experimentally by Joyce and Richards[64] and Brandli and Sievers.[65] A recent detailed theoretical treatment is given by Allen and Silberglitt.[66] The process involves an initial state with a photon at energy ω and the coupled electron-phonon system at zero temperature; the final state has an electron at energy $\mathcal{E}_1$, a hole at $\mathcal{E}_2$, and a phonon at energy ω_0. Energy conservation indicates that such a process only occurs when the photon frequency exceeds the phonon frequency; at that point a steplike increase in $\Gamma_1(\omega) = \tau^{-1}(\omega)$ is expected. Following Allen and Silberglitt[66] we write the frequency-dependent transport lifetime in the form

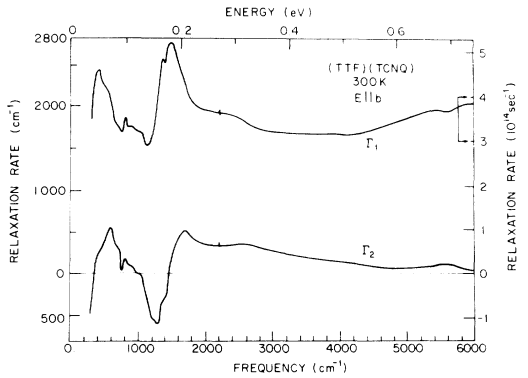

FIG. 27. Real and imaginary parts of the relaxation rate in TTF-TCNQ for $E \parallel b$ vs frequency from 300 to 6000 cm^{-1}.

$$\tau^{-1}(k, \omega) = 2\pi\omega^{-1}\int d\Omega\,(\omega - \Omega)\alpha^2F(k, \omega), \tag{40}$$

where

$$\alpha^2F(k, \omega) = g^2\sum_q B(q, \omega)\delta(\mathcal{E}_{k-q}) \tag{41}$$

is the product of the square of the electron-phonon matrix element (g^2) and the phonon density of states written in terms of the phonon spectral weight function $B(q, \omega)$. Assuming, initially, an Einstein phonon spectrum, we write

$$\tau^{-1}(k, \omega) = 2\pi(g^2/\omega)\int_0^\infty d\Omega\,(\omega - \Omega) \times[\delta(\Omega - \omega_0) - \delta(\Omega + \omega_0)], \tag{42}$$

$$\tau^{-1}(k, \omega) = \begin{cases} 0, & \omega < \omega_0, \\ 2\pi(g^2/\omega)(\omega - \omega_0), & \omega > \omega_0. \end{cases} \tag{43}$$

Thus, as expected, the Holstein process results in a steplike increase in $\tau_{\text{ph}}^{-1}(\omega)$ resulting from the onset of the process. This result disagrees with the calculation of Gutfreund *et al.*[62] but is in good agreement with a Golden-Rule calculation and with experiment in other systems.[64,65] The effect of phonon softening and the appearance of broad structure in $B(2k_F, \omega)$ is to further broaden the step. In no case does a resonant structure result.

We conclude that, within the context of conventional theory, the observed structure in $\sigma_1(\omega)$ is not attributable to resonance structure in the relaxation rate. On the other hand, the steplike structure predicted by Eq. (43) is not observed. The dynamic coupling of the conduction electrons to the C≡N modes may be considerably weaker than suggested by analysis of the bond-length changes in TCNQ salts. In addition, it appears likely that the models are just too simple. For example, in addition to a possible frequency dependence to τ_{sp}^{-1}, the gap function may be complex ($\Delta = \Delta_1 + i\Delta_2$). A reexamination of the data in terms of a Drude-Lorentz oscillator with a complex gap function yields structure reminiscent of that observed in strong-coupling superconductors.[67] However, a more detailed theoretical picture is required before these more subtle features of the optical data can be understood.

VIII. SUMMARY AND CONCLUSIONS

The infrared studies presented in this paper provide detailed experimental information on $\sigma_1(\omega)$ and $\epsilon_1(\omega)$ as a function of temperature for TTF-TCNQ. The results unambiguously establish the existence of the energy gap in the b-axis excitation spectrum. These infrared studies, together with earlier studies of dc[3-6] and microwave[7-10] transport properties provide strong evidence of a

coherent many-body state, having a current-carrying collective mode at zero frequency with single-particle excitations at higher frequencies. $\sigma_1^b(\omega)$ is thus qualitatively similar to that obtained from infrared studies of superconductors.

The detailed microscopic mechanism responsible for the important electronic properties of TTF-TCNQ is not yet clear. Many of the features are in agreement with expectations based on the developing understanding of the Peierls-Fröhlich sliding-mode state. On the other hand, BCS pairing in one dimension would also show the qualitative features seen in the data. The major questions which arise in this context relate to the remarkably high mean-field temperature and the apparent pinning of the current-carrying state at low temperatures. Evidently further experimental and theoretical work is required in order to provide the correct microscopic understanding.

Using the conventional mean-field result, $\hbar\omega_g = 3.5 k_B T_\rho$, with $\omega_g = 1050 \pm 100$ cm^{-1}, we obtain $T_\rho = 430$ K, in reasonable agreement with previous estimates of T_ρ from other measurements. One-dimensional fluctuations at temperatures below T_ρ smear the density of states such that the peak at the gap edge does not renormalize monotonically. The metal-insulator transition results from three-dimensional ordering with an associated pinning of the Fröhlich mode.

The *single-crystal* results for the frequency dependent b-axis conductivity can thus be summarized as follows:

(i) Zero frequency (dc)[3,4,6,68]: The conductivity is approximately 10^3 $(\Omega\,\mathrm{cm})^{-1}$ at room temperature increasing to values exceeding 10^4–10^5 $(\Omega\,\mathrm{cm})^{-1}$ near 58 K.

(ii) Microwave frequency (10^{10} GHz)[7,9,10]: The conductivity is approximately 10^3 $(\Omega\ \mathrm{cm})^{-1}$ at room temperature increasing to values exceeding 10^4–10^5 $(\Omega\ \mathrm{cm})^{-1}$ near 58 K. At both dc and microwave frequencies it appears likely that the peak conductivities are defect limited so that the intrinsic value may be even higher. However, a peak value exceeding 2×10^4 $(\Omega\ \mathrm{cm})^{-1}$ is conservative.

(iii) Infrared frequencies (50–10 000 cm^{-1})[2,11–13]: There is an energy gap with magnitude $\hbar\omega_g \sim 0.14$ eV above which the single-particle conductivity is Drude-like with a well-defined plasma frequency $\hbar\omega_p \sim 1.2$ eV. Except for the structure near 1400 cm^{-1}, the conductivity and dielectric function are well described by a Lorentzian oscillator with resonant frequency ω_g, strength ω_p^2, and full width at half maximum τ_{sp}^{-1}. The temperature dependence is weak with the single-particle scattering time varying by about a factor of 2 between 300 and 60 K.

(iv) Visible frequencies (10 000–37 000 cm^{-1})[11–13]: The conductivity arises from interband transitions and intramolecular electronic transitions. The conductivity along the b axis is still five to ten times greater than along the a axis.

The *thin-film* results[1] for the frequency-dependent conductivity extend the single-crystal results as follows:

(a) Far-infrared frequencies (20–200 cm^{-1}): The conductivity is relatively small but weakly metallic (increasing with decreasing temperature) above the 58-K metal-insulator transition. At lower temperatures the over-all level of the conductivity decreases as the pinned mode appears, centered in all films measured to date at 80 cm^{-1}. The low-temperature data show no evidence of a smaller energy gap with magnitude $E_g/k_B \sim 150$ K, as inferred from the temperature dependence of the magnetic susceptibility and transport properties below 58 K. We conclude that the optical transitions associated with this smaller gap have little or no oscillator strength.

(b) Infrared frequencies (200–4000 cm^{-1}): The energy gap is present at all temperatures. Reduction of the temperature sharpens the structure, but the metal-insulator transition is all but invisible at these frequencies. These results are sketched graphically in Fig. 28, which is drawn to qualitatively describe the frequency dependence of $\sigma_1^b(\omega)$ at 300, 60, and 4.2 K.

Much of the discussion surrounding the study of TTF-TCNQ and related systems has centered on the dc electrical conductivity. However, it is now generally agreed that the intrinsic conductivity exceeds 10^4 $(\Omega\ \mathrm{cm})^{-1}$, and there is strong evidence that the peak value is approximately 10^5 $(\Omega\ \mathrm{cm})^{-1}$

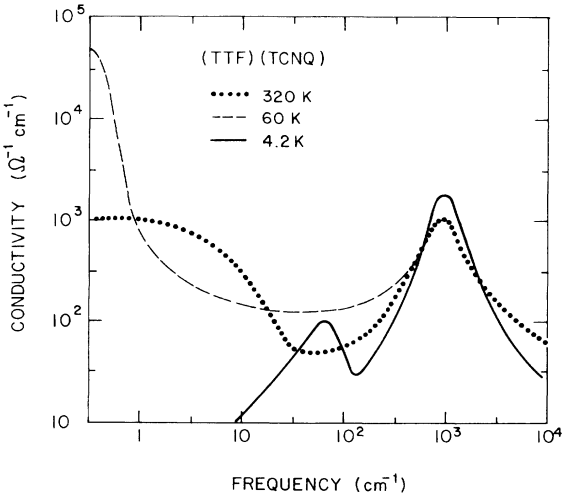

FIG. 28. Schematic picture of the real part of the conductivity of TTF-TCNQ, at three temperatures, vs frequency from 0.3 to 10^4 cm^{-1} (microwave to near-ir).

both at dc[4] and microwave[9] frequencies. The sensitivity of the one-dimensional conductor to impurities and defects has been established.[4,7] However, it is most important to view the dc and microwave conductivities in the context of our overall experimental knowledge of $\sigma_1(\omega)$ and $\epsilon_1(\omega)$ as presented in this paper and in our earlier work.[1,2] TTF-TCNQ is not a simple metal. There is an energy gap; the dc conductivity arises from an extremely narrow collective-mode peak centered at zero frequency in this quasi-one-dimensional system.

ACKNOWLEDGMENTS

We would like to thank Professor E. R. Nixon and Professor E. Burstein of the University of Pennsylvania and Professor A. J. Sievers of Cornell University for the use of their facilities. We thank P. Nigrey for careful sample preparation and Dr. G. M. T. Foley for aid in constructing the far-infrared reflectance insert. Finally we gratefully acknowledge stimulating discussions with Professor L. Gorkov. Work at Cornell supported by the Energy Research and Development Administration through contract No. AT(11-1)-3151.

---

*Present address: Dept. of Physics, Ohio State University, Columbus, Ohio 43210.

†Present address: Physics Lab. III, Technical University of Denmark, DK-2800 Lyngby, Denmark.

‡Research supported by the NSF through the Laboratory for Research on the Structure of Matter and Grant No. GH-39303 and by the Advanced Research Projects Agency through Grant No. DAHC-15072-C-0174.

[1]D. B. Tanner, C. S. Jacobsen, A. F. Garito, and A. J. Heeger, Phys. Rev. Lett. 32, 1301 (1974).

[2]C. S. Jacobsen, D. B. Tanner, A. F. Garito, and A. J. Heeger, Phys. Rev. Lett. 33, 1559 (1974).

[3]L. B. Coleman, M. J. Cohen, D. J. Sandman, F. C. Yamagishi, A. F. Garito, and A. J. Heeger, Solid State Commun. 12, 1125 (1973).

[4]Marshall J. Cohen, L. B. Coleman, A. F. Garito, and A. J. Heeger, Phys. Rev. B 10, 1298 (1974).

[5]John Ferraris, D. O. Cowan, V. Walatka, Jr., and J. H. Perlstein, J. Am. Chem. Soc. 95, 948 (1973).

[6]R. P. Groff, A. Suna, and R. E. Merrifield, Phys. Rev. Lett. 33, 418 (1974).

[7]S. K. Khanna, E. Ehrenfreund, A. F. Garito, and A. J. Heeger, Phys. Rev. B 10, 2205 (1974).

[8]S. K. Khanna, A. F. Garito, A. J. Heeger, and R. C. Jaklevic, Solid State Commun. 16, 667 (1975).

[9]Michael Cohen, S. K. Khanna, W. J. Gunning, A. F. Garito, and A. J. Heeger, Solid State Commun. 17, 367 (1975).

[10]J. P. Ferraris and T. Finnegan, Solid State Commun. (to be published); preliminary results in Bull. Am. Phys. Soc. 20, 466 (1975).

[11]A. A. Bright, A. F. Garito, and A. J. Heeger, Solid State Commun. 13, 943 (1973).

[12]A. A. Bright, A. F. Garito, and A. J. Heeger, Phys. Rev. B 10, 1328 (1974).

[13]P. M. Grant, R. L. Greene, G. C. Wrighton, and A. Castro, Phys. Rev. Lett. 31, 1311 (1973).

[14]J. C. Scott, A. F. Garito, and A. J. Heeger, Phys. Rev. B 10, 3131 (1974).

[15]T. Wei, S. Etemad, A. F. Garito, and A. J. Heeger, Phys. Lett. A 45, 269 (1973).

[16]R. A. Craven, M. B. Salamon, G. DePasquali, R. M. Herman, G. Stucky, and A. Schultz, Phys. Rev. Lett. 32, 770 (1974).

[17]F. Denoyer, R. Comes, A. F. Garito, and A. J. Heeger, Phys. Rev. Lett. 35, 445 (1975); S. Kagoshima, H. Anzai, K. Kajimura, and T. Ishiguro, J. Phys. Soc. Jpn. 39, 1143 (1975); R. Comes, S. M. Shapiro, G. Shirane, A. F. Garito, and A. J. Heeger, Phys. Rev. Lett. 35, 1518 (1975).

[18]R. E. Peierls, *Quantum Theory of Solids* (Clarendon, Oxford, 1955), p. 108.

[19]H. Frölich, Proc. R. Soc. A 223, 296 (1954).

[20]J. R. Schrieffer, in *Collective Properties of Physical Systems*, edited by B. Lundquist and S. Lundquist (Academic, New York, 1973), p. 142.

[21]P. A. Lee, T. M. Rice, and P. W. Anderson, Solid State Commun. 14, 703 (1974).

[22]Y. A. Bychkov, Zh. Eksp. Teor. Fiz. 65, 427 (1973) [Sov. Phys.-JETP 38, 209 (1974)].

[23]V. L. Berezinskii, Zh. Eksp. Teor. Fiz. 65, 1251 (1973) [Sov. Phys.-JETP 38, 620 (1974)].

[24]A. A. Gogolin, V. I. Mel'nikov, and E. I. Rashba, Zh. Eksp. Teor. Fiz. (to be published).

[25]John Bardeen, Solid State Commun. 13, 357 (1973).

[26]David Allender, J. W. Bray, and John Bardeen, Phys. Rev. B 9, 119 (1974).

[27]A. Luther and I. Peschel, Phys. Rev. Lett. 32, 992 (1974).

[28]Daniel C. Mattis, Phys. Rev. Lett. 32, 714 (1974).

[29]H. Fukuyama, T. M. Rice, and C. M. Varma, Phys. Rev. Lett. 33, 305 (1974).

[30]Bruce R. Patton and L. J. Sham, Phys. Rev. Lett. 31, 631 (1973).

[31]Bruce R. Patton and L. J. Sham, Phys. Rev. Lett. 33, 638 (1974).

[32]J. B. Sokoloff, Solid State Commun. 16, 375 (1975).

[33]M. J. Rice, Solid State Commun. 16, 1285 (1975).

[34]J. B. Torrance and D. F. Nicoli, Bull. Am. Phys. Soc. 19, 336 (1974).

[35]P. Chaudhari, B. A. Scott, R. B. Laibowitz, Y. Tomkiewitz, and J. B. Torrance, Appl. Phys. Lett. 24, 439 (1974).

[36]T. O. Poehler, A. N. Bloch, J. P. Ferraris, and D. O. Cowan, Solid State Commun. 15, 337 (1974).

[37]J. E. Eldridge (unpublished); preliminary results in Bull. Am. Phys. Soc. 20, 495 (1975).

[38]L. B. Coleman, J. A. Cohen, A. F. Garito, and A. J. Heeger, Phys. Rev. B 7, 2122 (1973).

[39]See, for example, F. Wooten, *Optical Properties of Solids* (Academic, New York, 1972), Appendix A.

[40]Leigh Hunt Palmer and M. Tinkham, Phys. Rev. 165, 588 (1968).

[41]L. N. Hadley and D. M. Dennison, J. Opt. Soc. Am. 37, 451 (1947).

[42]A complete discussion with all the details is given in

C. S. Jacobsen, thesis (Technical University of Denmark, DK-2800 Lyngby, Denmark) (unpublished).
[43]J. C. Maxwell-Garnett, Philos. Trans. R. Soc. Lond. 203, 385 (1904); 205, 237 (1906).
[44]L. Gentzel and T. P. Martin, Phys. Status Solidi 51, 91 (1972).
[45]A. S. Barker, Jr., Phys. Rev. B 7, 2057 (1973).
[46]D. B. Tanner, A. J. Sievers, and R. A. Buhrman, Phys. Rev. B 11, 1330 (1975).
[47]B. Lunelli and C. Pecile, J. Chem. Phys. 52, 2375 (1970).
[48]I. G. Nolt, R. D. Kirby, C. D. Lytle, and A. J. Sievers, Appl. Opt. 8, 309 (1969).
[49]S. K. Khanna, A. A. Bright, A. F. Garito, and A. J. Heeger, Phys. Rev. B 10, 2139 (1974).
[50]P. Bruesch, S. Strassler, and H. R. Zeller, Phys. Rev. B 12, 219 (1975).
[51]J. J. Ritsko, D. J. Sandman, A. J. Epstein, P. C. Gibbons, S. E. Schnatterly, and J. Fields, Phys. Rev. Lett. 34, 1330 (1975).
[52]C. G. Kuper, Proc. R. Soc. Lond. A 227, 214 (1955).
[53]P. A. Lee, T. M. Rice, and P. W. Anderson, Phys. Rev. Lett. 31, 462 (1973).
[54]H. R. Zeller, Bull. Am. Phys. Soc. 19, 195 (1974).
[55]P. Brüesch and H. R. Zeller, Solid State Commun. 14, 1037 (1974).
[56]L. J. Buravov and I. F. Shchegolev, Prib. Tekh. Eksp. 2, 171 (1971).
[57]R. C. Jaklevic and R. B. Saillant, Solid State Commun. 15, 307 (1974).
[58]L. B. Coleman, C. R. Fincher, Jr., A. F. Garito, and A. J. Heeger, Phys. Status Solidi (to be published). The single crystal results imply an intrinsic pinning frequency of 2 cm^{-1} and a collective mode oscillator strength of 250 ± 50 cm^{-1}.
[59]S. Etemad, T. Penney, and E. M. Engler, Bull. Am. Phys. Soc. 20, 496 (1975); S. Etemad (unpublished).
[60]W. N. Hardy, A. J. Berlinsky, and L. Weiler, Bull. Am. Phys. Soc. 20, 466 (1975).
[61]A. John Berlinsky, James F. Carolan, and Larry Weiler, Solid State Commun. 15, 795 (1974).
[62]H. Gutfreund, B. Horowitz, and M. Weger, Solid State Commun. 15, 849 (1974); see also B. Horowitz, M. Weger, and H. Gutfreund, Phys. Rev. B 9, 1246 (1974).
[63]T. Holstein, Phys. Rev. 96, 535 (1954).
[64]R. R. Joyce and P. L. Richard, Phys. Rev. Lett. 24, 1007 (1970).
[65]G. Brandli and A. J. Sievers, Phys. Rev. B 5, 3550 (1972).
[66]Philip B. Allen and Richard Silberglitt, Phys. Rev. B 9, 4733 (1974).
[67]D. J. Scalapino, J. R. Schrieffer, and J. W. Wilkins, Phys. Rev. Lett. 10, 336 (1963); Phys. Rev. 148, 263 (1966).
[68]D. Jerome, W. Muller, and M. Weger, J. Phys. Lett. (Paris) 35, 77 (1974).